ELSEVIER

Contents lists available at ScienceDirect

Tectonophysics

journal homepage: www.elsevier.com/locate/tecto



Active fault map and paleoseismology results from the Aceh Fault in North Sumatra, Indonesia: Unravelling faulting dynamics along the Great Sumatran Fault system

Gayatri Indah Marliyani ^{a,*}, Yann Klinger ^b, Aulia Kurnia Hady ^c, Agung Setianto ^a, Wenqian Yao ^b, Hurien Helmi ^d, Telly Kurniawan ^e, Retno Agung Prasetyo Kambali ^e, Zulham Sugito ^e, Abdi Jihad ^e, Yosi Setiawan ^e, Andi Azhar Rusdin ^e, Jimmi Nugraha ^e, Supriyanto Rohadi ^e, Rahmat Triyono ^e, Dwikorita Karnawati ^{a,e}

- ^a Geological Engineering Department, Universitas Gadjah Mada, Jl Grafika No 2, Yogyakarta, Indonesia
- ^b Université Paris Cité, Institut de Physique du Globe de Paris, CNRS, 1 Rue Jussieu, Paris, France
- ^c Department of Energy and Mineral Resources of NAD Province, l. Teuku Nyak Arief No.195, Banda Aceh, Indonesia
- ^d Geological Engineering Department, Institut Teknologi Nasional Yogyakarta, Jl. Babarsari, Tambak Bayan, Yogyakarta, Indonesia
- ^e Meteorology, Climatology, and Geophysical Agency, Jl. Angkasa I No. 2, Kemayoran, Jakarta Pusat, Indonesia

ARTICLE INFO

Keywords: Aceh fault Sumatra Earthquake Paleoseismology Active tectonics Seismic hazards

ABSTRACT

The Aceh Fault, a major strike-slip fault forming the northernmost segment of Great Sumatran Fault, exhibits recent faulting through prominent scarps along its 250-km length. Running northwest-southeast, it traverses northwestern Sumatra from Tripa to Banda Aceh, a city of over 268,000 residents that is more commonly associated with the 2004 tsunami, but also lies directly on this active fault zone. Understanding the earthquake rupture history, including pre-instrumental events, is essential to characterize long-term seismic patterns and to assess associated hazards. We investigated the fault using 8-m resolution DEM (DEMNAS) for the entire fault zone, 15-cm resolution lidar DEM for selected areas, field mapping, and paleoseismology. Two paleoseismic trenches excavated in the Geumpang area reveal evidence of at least three ground-rupturing earthquakes over the past ~1000 years. Event timing was constrained by radiocarbon analysis of detrital charcoal, providing sufficient chronological control to identify two well-dated events and one older event with lower precision. These results confirm that the Aceh Fault is active, delineate its surface trace, and offer the first detailed record of prehistoric earthquakes along this fault. This information contributes to improved seismic hazard mapping and a clearer understanding of tectonic risk in the Banda Aceh region.

1. Introduction

The Aceh Fault, located in western Indonesia, constitutes the northernmost part of the Great Sumatran Fault System (GSF in Fig. 1). Evidence of recent faulting is apparent in the topography, as indicated by the presence of prominent fault scarps that cut through youthful geomorphic features like river terraces and channels along the 250-kmlong fault (Hady, 2020; Hady and Marliyani, 2020; Sieh and Natawidjaja, 2000). However, there have been no documented recent notable earthquakes apart from minor ones, such as those with magnitudes of M4 to M5, which occurred in 2020 (BMKG earthquake catalogue, https://repogempa.bmkg.go.id/). This fault strikes in a

northwest-southeast (NW-SE) direction, spanning the northwestern region of Sumatra Island, starting from the Tripa region and passing through the outskirts of Banda Aceh city (Fig. 1). Banda Aceh is the provincial capital of Nanggaroe Aceh Darussalam and is home to over 268,000 residents. The city was completely devastated by the 2004 Indian Ocean tsunami, triggered by the massive Sumatra-Andaman earthquake, revealing its double vulnerability to earthquake and tsunami hazards.

Tectonically, the Aceh Fault is a major dextral strike-slip fault system that accommodates a significant portion of the forearc motion above the Andaman-Sumatran subduction zone, with long-term slip rates on the order of tens of millimeters per year. This displacement is distributed

E-mail address: gayatri.marliyani@ugm.ac.id (G.I. Marliyani).

^{*} Corresponding author.

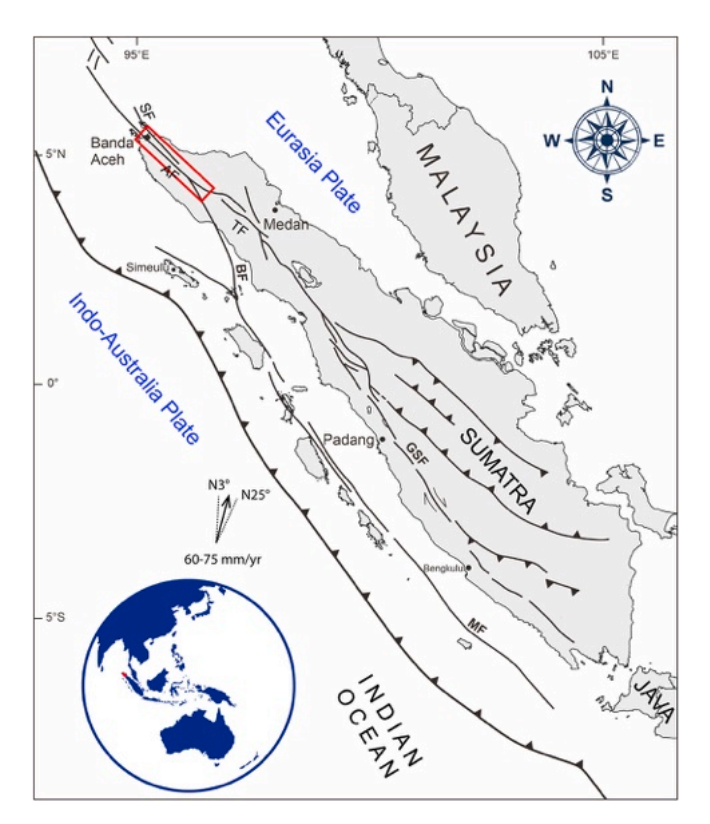


Fig. 1. Tectonic framework map of the Great Sumatran Fault (GSF) system highlighting major fault sections in northern Sumatra, including the Aceh Fault (AF), Seulimeum Fault (SF), Mentawai Fault (MF), Tripa Fault (TF), and Batee Fault (BF). The red box outlines the current study area. Fault traces and structural interpretations are adopted from Bellier and Sebrier (1995), while plate convergence direction and velocity are derived from DeMets et al. (1990) and McCaffrey (2000). (For interpretation of the references to colour in this figure legend, the reader is referred to the web version of this article.)

heterogeneously along strike, with both creeping and locked sections influencing the pattern of strain accumulation and release as elaborated in Section 2. The absence of significant earthquakes along this 250-kmlong section since the beginning of instrumental seismicity implies a potential of increased seismic risk for this area, as suggested by Bellier et al. (1997) and Sieh and Natawidjaja (2000). However, to date the potential danger posed by this fault has been mostly overlooked, as most attention is focused on the threat posed by nearby subduction events, which can be devastating, as seen during the Aceh tsunami in 2004 (Rofi et al., 2006).

Building the most complete history of earthquake rupture events is key to understanding the earthquake patterns, both in time and space, for specific active fault systems such as the GSF. However, instrumental seismicity is often too limited, especially for large magnitude events, due to long recurrence intervals between earthquakes relative to human history. Hence, the paleoseismology, which involves studying past earthquakes by examining evidence of faulting and establishing earthquake chronology, is instrumental to build a representative view of the long-term seismicity for a given fault system (McCalpin et al., 2023; Marliyani and Grant, 2016; Pinzon et al., 2024).

In this study, we map the Aceh Fault using a combination of remote sensing data and field observations. We also conducted paleoseismological investigations along the fault to bracket the timing of the most recent earthquakes. Eventually, this study should not only improve the quality of the active fault map in Sumatra, but it should also provide valuable insights into the seismic history of the northern part of the GSF, ultimately contributing to the development of a more accurate seismic hazard map for the region.

2. Tectonic and geological setting of Aceh Fault

The tectonics of the Sumatra Island is dominated by the oblique subduction of the Indo-Australian oceanic plate beneath the Eurasian continental plate. The convergence rate normal to the trench along the Sumatra subduction zone decreases from approximately 50–60 mm/year in the southern section to less than 30 mm/year toward the northern end near the Andaman region, reflecting variations in plate motion and slab geometry along strike (e.g., Kreemer et al., 2003; Bock et al., 2003; McCaffrey, 2009; Tregoning, 2002). The obliquity angle along the Sumatra subduction zone varies significantly along strike, increasing from nearly orthogonal convergence (~10°) in the southern segment to highly oblique convergence exceeding ~30° toward the northern segment, leading to greater partitioning of slip onto the Sumatran Fault in the north (Guzmán-Speziale, 2024).

The deformation associated with the subduction is then accommodated through the partitioning of the displacement between the actual subduction that accounts for the displacement perpendicular to the subduction trench and the continental GSF that accounts for the part of displacement parallel to the trench. Hence, the horizontal motion accommodated by the GSF is dominated by right-lateral strike-slip, which extends across Sumatra Island and closely parallels the direction of the subduction trench (McCaffrey, 2009; Genrich et al., 2000). Another fault that accommodates some of the horizontal motion associated with the subduction is the Mentawai Fault. In northwestern Sumatra, this fault connects to the GSF via the Batee Fault (Diament et al., 1992; Berglar et al., 2017)(Fig. 1). The Aceh Fault begins ~40 km to the southeast from the junction of the Batee Fault and the GSF. From there, the Aceh Fault continues as a single fault for 75 km before bifurcating into two separate faults, with the Seulimeum Fault branching off from the GSF to the northeast direction.

Paleoseismic investigations along the Great Sumatran Fault (GSF) provide important context for understanding rupture recurrence and segmentation behavior. Early trenching efforts on the southern GSF documented surface-rupturing events in late Holocene deposits, highlighting the active and hazardous nature of the fault (e.g., Bellier et al., 1997). Further north, studies by Tsutsumi et al. (2022) at Lamtamot on the Seulimeum Fault revealed at least three surface-rupturing events since ~1280 CE, supported by geomorphic mapping and site characterization (Yanis et al., 2022). These findings complement broader neotectonic work on GSF segmentation and slip behavior (Sieh and Natawidjaja, 2000). In the southern part of the GSF, recent geological studies by Natawidjaja et al. (2017) have refined slip rate estimates using right-lateral offsets of river channels incised into the Ranau Tuff. The Kumering Fault records a slip rate of 10.4 \pm 1.5 mm/yr, while the West Semangko Fault yields 6.8 ± 1.8 mm/yr. The East Semangko Fault is inferred to slip at ~3.6 mm/yr, giving an aggregate slip rate of ~15 mm/yr across the southern Sumatran Fault Zone, consistent with geodetic measurements. Reported recurrence intervals surface-rupturing earthquakes along various sections of the GSF typically range from 60 to 200 years, with variability attributed to differences in slip rate, fault geometry, and segment behavior. In contrast, paleoseismic constraints on the Aceh Fault remain limited. This study contributes new paleoseismic data from this northern section, providing a critical comparison point to better understand along-strike variability in earthquake recurrence along the GSF.

Although the Aceh Fault has shown recent seismic activity, its slip characteristics, as well as those of the Great Sumatran Fault (GSF) in general, are not well understood. A frequently referenced slip rate for the northern GSF is 38 mm/year, a number proposed by McCaffrey et al. (2000), who used a geodetic method. McCaffrey et al. (2000) adopted Fitch (1972) model which suggests that the forearc plate, bounded by the trench and transcurrent fault, behaves rigidly, allowing long-term slip rates to be inferred from fault geometry, slip vectors, and plate motion vectors. In contrast, a study conducted by Ito et al. (2012) who deployed the AGNeSS GPS array in the area recorded a right-lateral

elastic strain accumulation rate of 20 ± 6 mm/year along the Aceh Fault from 2005 to 2010. Tong et al. (2018) found the northern part of the Sumatran Fault, particularly the Aceh segment, exhibits significant aseismic creep behavior. Using InSAR data, the study identified creep rates of up to approximately 20 mm/year along a ~ 100 km stretch of the fault. This value represents a substantial fraction of the long-term slip rate estimated for this segment (20–38 mm/yr), indicating that creep may account for more than half of the total interseismic deformation in some areas. This characteristic has important implications for how strain accumulates and is released along the fault. In particular, if aseismic slip is active near the trench site, we would expect subtle but

persistent deformation to be recorded in the shallow stratigraphy. Conversely, the absence of such features can also provide meaningful insight into how creep is distributed along strike and with depth. The variation of slip distribution along strike shown by that study indicates spatial variability in strain release. While the central creeping section accumulates seismic moment at about half the rate of adjacent locked segments, it still poses a notable hazard. Moreover, the researchers observed signs of temporal deceleration in the creep rate, potentially influenced by stress changes from nearby seismic events. This creeping behavior may reduce the likelihood of sudden rupture within the segment itself but could increase stress transfer to neighboring locked

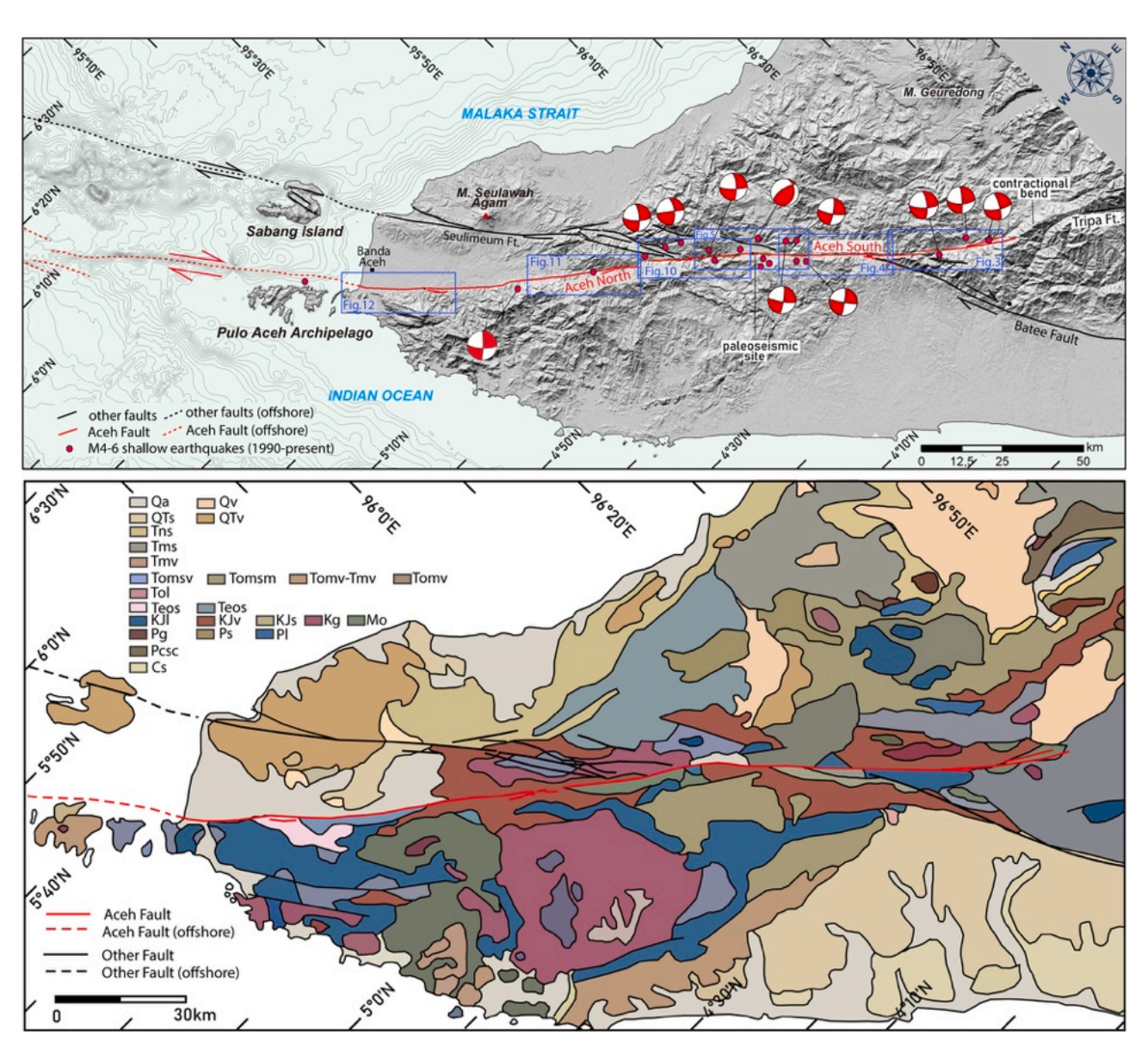


Fig. 2. Upper: seismotectonic map showing the distribution of shallow, moderate-magnitude earthquakes (M4–6) associated with active faulting in the Aceh Fault zone. Earthquake data are from the Global CMT catalogue (https://www.globalcmt.org/CMTsearch.html). The map incorporates shaded topography from the 8-m resolution DEMNAS (https://tanahair.indonesia.go.id/demnas/#/) and 100-m bathymetric contours from BATNAS (https://tanahair.indonesia.go.id/demnas/#/batnas). Blue rectangles indicate the areas shown in the following figures. Red lines denote the Aceh Fault; black lines indicate other mapped faults in the region. Lower: Regional geological map (1:1000,000) from Gafoer et al. (1996), showing the Aceh Fault transecting a geologically complex region composed of Jurassic-Cretaceous basement rocks, Oligocene deep-marine deposits, and turbiditic and Quaternary sedimentary sequences. Qa: Quaternary alluvium, Qv:Quaternary volcanics, Qts: Plio-Pleistocene sediments, Qtv: Plio-Pleistocene volcanics, Tns: Mio-Pliocene sediments, Tms: Miocene shallow marine sediments, Toms: Oligo-Miocene tuffaceous sediments, Tomsm: Oligo-Miocene intrusions, Teos: Eocene-Oligocene shallow marine-terrestrial sediments, Kjl: Jurassic-Cretaceous carbonate rocks, KJs: Jurassic-Cretaceous sediments, Kjv: Jurassic-Cretaceous volcanic rocks, Rg: Cretaceous Granite, Mo: Jurassic-Cretaceous Ophiolite complex' Pg: Permian Granite, Ps: Permian clastic rocks, Pl: Permian carbonate rocks, PCsc: Permo-Caroniferous Clastic Rocks, Cs: Carboniferous sediments. (For interpretation of the references to colour in this figure legend, the reader is referred to the web version of this article.)

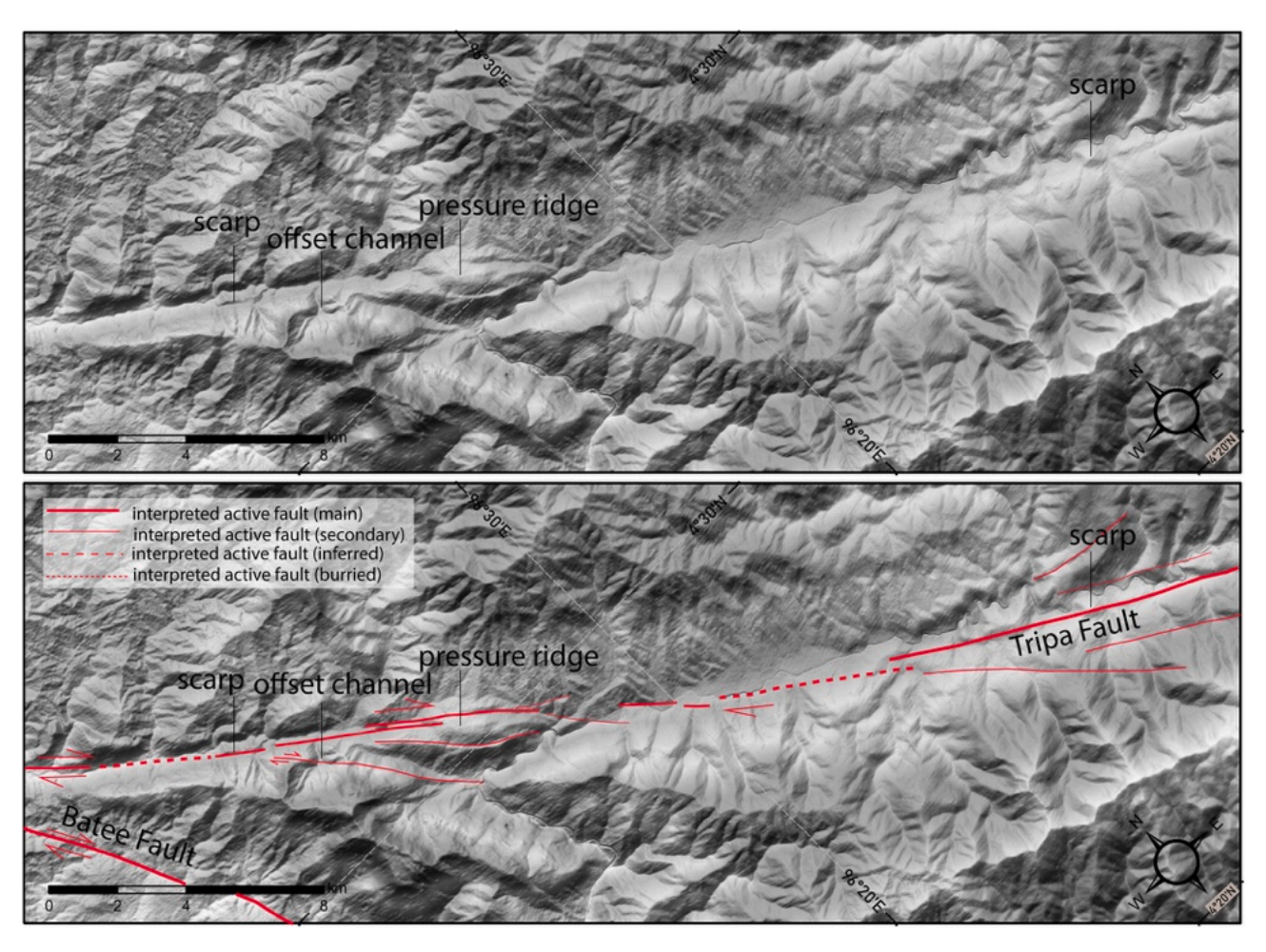


Fig. 3. Detailed geomorphic map of the southeasternmost segment of the Aceh Fault near its intersection with the NW-SE trending Batee Fault. Tectonic landforms such as scarps, offset streams, and pressure ridges help define the active fault trace. A pressure ridge demarcates the boundary between this segment and the Tripa Fault to the northeast. Hillshaded base layer is derived from the 8-m DEMNAS dataset (https://tanahair.indonesia.go.id/demnas/#/). Refer to Fig. 2 for the regional location.

zones, making it a critical consideration in regional earthquake hazard assessments.

The Aceh Fault is evident in the topography, appearing as a prominent, straight fault scarp with a total length of 250 km. There have been various hypotheses regarding whether this entire 250 km stretch should be treated as a single fault or if it should be regarded as multiple distinct sections. Sieh and Natawidjaja (2000) considered the entire 250 km fault as a single section, whereas in the National Earthquake Hazard Map of Indonesia, the fault is divided into three sections: Aceh North, Aceh Central and Aceh South (Pusat Studi Gempa Nasional, 2017). Meanwhile, Hady and Marliyani (2020) opted to divide the fault into seven distinct sections based on detailed active fault mapping using highresolution topographic data, including ~8-m DEMNAS and sub-meter UAV-derived DEMs, combined with tectonic geomorphology indicators such as fault bends, step-overs, and terminations, as well as field observations confirming consistent right-lateral strike-slip motion. Given that strike-slip faults rarely rupture continuously over such long distances, and that empirical studies suggest rupture lengths typically range between 50 and 200 km depending on fault geometry and stress conditions (Mignan et al., 2015), it is more reasonable to treat the fault as a series of shorter segments that could link together in larger ruptures. This segmentation aligns with physical constraints on rupture propagation, such as fault step-overs and bends, which often arrest seismic ruptures. Therefore, modeling the fault as multiple distinct sections provides a more realistic framework for assessing seismic hazard. The Aceh Fault is separated from Tripa Fault section in the southeast by a \sim

9 km wide restraining band (Sieh and Natawidjaja, 2000; Pusat Studi Gempa Nasional, 2017) (Fig. 1). To the northeast of the Tripa region, the fault passes through the mountainous areas of Geumpang, Tangse, and Jantho. In the northwestern part, the Aceh Fault traverses the relatively flat terrain near Banda Aceh, extends offshore, and converges with the Andaman Nicobar Fault (Curray et al., 1979; Singh et al., 2013; Jourdain et al., 2016) (Fig. 1).

The Aceh Fault cuts through a complex of Jurassic-Cretaceous basement rocks, predominantly made up of metamorphic rocks, which are prominently exposed in the elevated regions (Fig. 2) (Bennett et al., 1981). Overlying the basement rocks are sequences of Oligocene deep marine deposits, followed by volcanic and turbiditic sediments. More recent volcanic material then covers these rock units. The lowland area of the Krueng Aceh basin is filled with young alluvial deposits consisting of silt to gravel sediments (Bennett et al., 1981; Moechtar et al., 2009). The strike-slip movement of the Aceh Fault has led to the formation of several pull-apart basins along the fault. These basins, such as those in the Tangse and Geumpang areas, are filled with Quaternary alluvial deposits, as indicated in the published geological map of the region (Bennett et al., 1981).

3. Methods

3.1. Active fault mapping

We conducted a tectonic geomorphological analysis using Digital

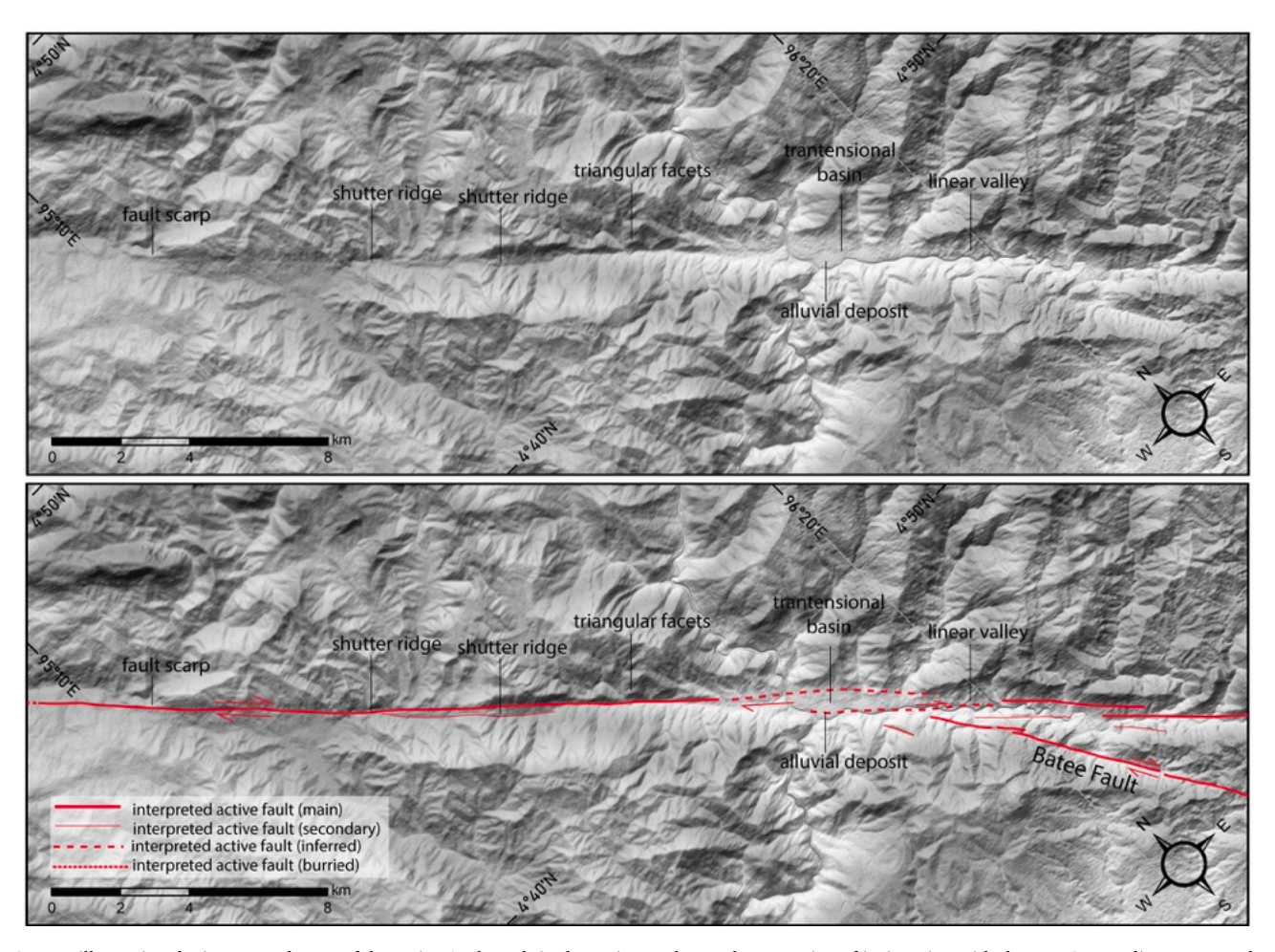


Fig. 4. Map illustrating the interpreted trace of the active Aceh Fault in the region to the northwest region of its junction with the NW–SE-trending Batee Fault. The fault trace was delineated based on the identification of key tectonic geomorphic indicators, including fault scarps, linear valleys, shutter ridges, and triangular facets, which are characteristic of active strike-slip faulting. These geomorphic expressions were mapped through detailed analysis of topographic features visible on a hillshaded Digital Elevation Model (DEM) derived from the 8-m resolution national DEM (DEMNAS), produced by the Geospatial Information Agency of Indonesia (https://tanahair.indonesia.go.id/demnas/#/). For regional context, the location of this map area is indicated in Fig. 2.

Elevation Model (DEM) data at three different resolutions: first, the national 8-m resolution DEM obtained from DEMNAS (available at http://tides.big.go.id/DEMNAS/) covering the entire study area; second, a 15-cm resolution DEM computed from UAV drone aerial photographs; and third, a 10-cm lidar DEM covering only a few selected locations. The primary target was to detect evidence of surface faulting, and more specifically fault scarps where they might intersect with Quaternary deposits, and thus having favourable conditions for paleoseismic trenching.

Given the strike-slip nature of the fault, deformation is evidenced by the lateral displacement of geomorphic features like river channels, river terraces, and ridges. While mapping systematically geomorphic offsets, we paid special attention to lateral consistency of successive observations to ensure that we do not overinterpret natural complexity of landforms as tectonic related deformation.

3.2. Paleoseismic trenching

After identifying suitable sites through active fault mapping, we excavated two trenches using a backhoe. Each trench reached a depth of approximately 1.5 m and extended to length of respectively 50 and 40 m. These trenches aimed to delineate the primary fault zone at the site. To prepare the trench walls for analysis, we manually cleaned them using scraping tools and shovels. Subsequently, we gridded the walls with horizontal lines spaced at half-meter intervals to serve as reference

points. We photographed the trench walls and processed these images into composite photo-mosaics using Structure from Motion techniques, creating a base map for documenting stratigraphic and faulting relationships.

As part of our analysis, we documented the visible layers of sediment within the trench walls, marked the fault's traces, identified any signs of surface ruptures, and pinpointed the positions of samples collected for age dating on the trench wall maps (logs). To aid discussions, we assigned numerical designations to the various stratigraphic units, with the numbers ascending in correspondence to both depth and age.

We collected a total of 29 wood and charcoal samples from both trenches for radiocarbon (14C) dating (Walker, 2005). Prioritizing samples based on their potential contribution to developing the event history, sample quality, and the stratigraphic context, 13 charcoal samples were analyzed at the W. M. Keck Carbon Cycle Accelerator Mass Spectrometry Laboratory at the University of California, Irvine. To calibrate the dates, we used the IntCal13 calibration curve (Reimer et al., 2013a, 2013b; Reimer, 2020) and further employed Oxcal software to construct an age model for the successive earthquakes recognized in the trenches (Lienkaemper and Ramsey, 2009; https://c14.arch.ox.ac.uk/).

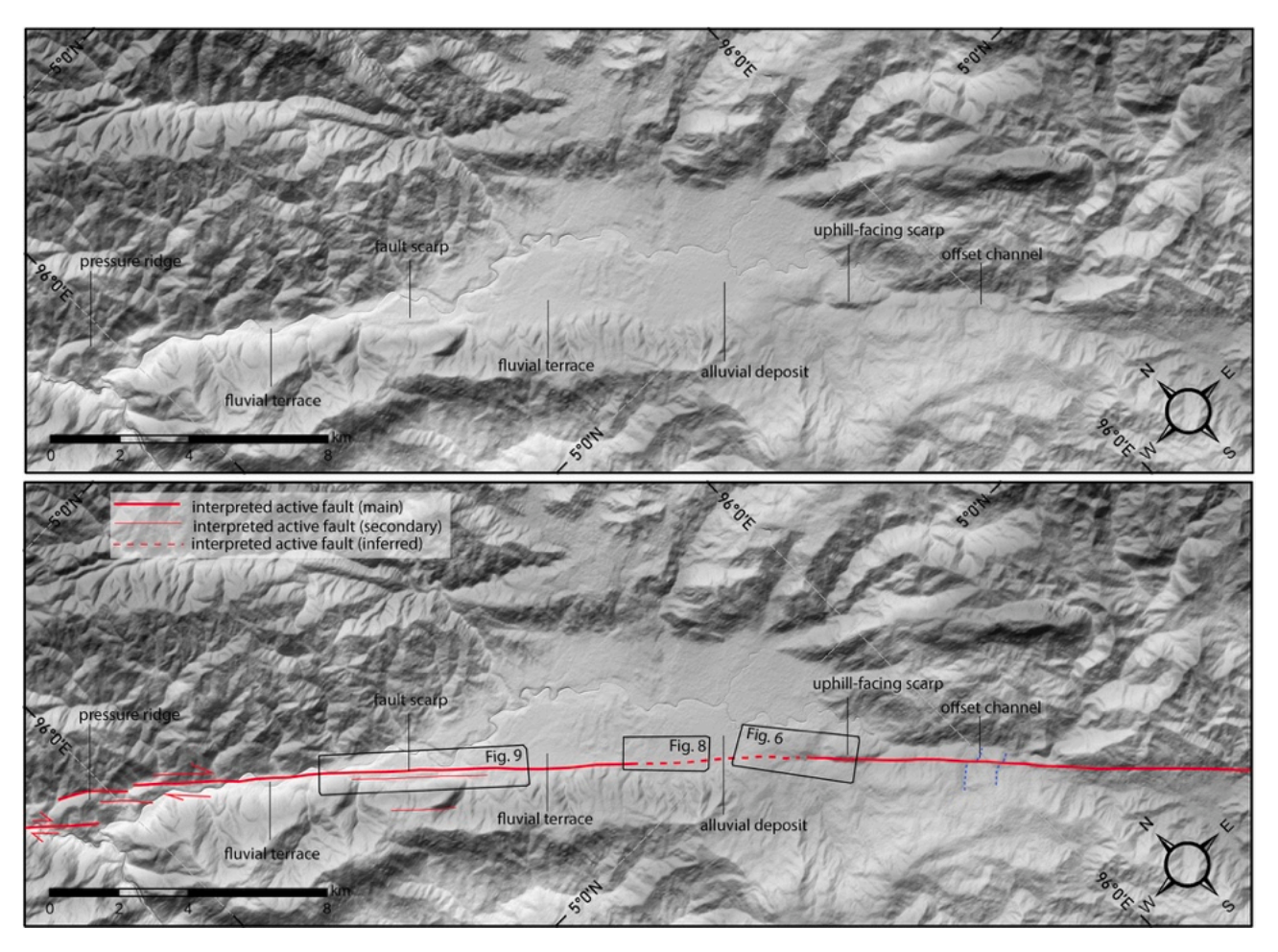


Fig. 5. Geomorphic interpretation map of the Aceh Fault near Geumpang Village, showing tectonic features including scarps, deflected channels (blue dotted lines), and displaced fluvial terraces. The hillshaded relief is based on 8-m DEMNAS data (https://tanahair.indonesia.go.id/demnas/#/), while black polygons represent the extent of 15-cm resolution lidar datasets. Location corresponds with the area outlined in Fig. 2. (For interpretation of the references to colour in this figure legend, the reader is referred to the web version of this article.)

4. Results

4.1. Active fault map

Identifying evidence of active faulting in the mountainous areas of Sumatra is challenging due to the dense vegetation, which obstructs any landscape perspective unless it has been cleared. In addition, the deforested areas are typically immediately used for agriculture, rice paddies, or cattle herding, and thus are significantly altered by human activities.

The 8-m resolution DEM from the DEMNAS data allowed us to identify the main cumulative topographic features and lineaments associated with the active faulting along the Aceh Fault. However, due to its resolution, those data cannot capture small-scale topographic features that would correspond to the most recent deformation. Hence, the 10-cm resolution lidar data acquired by drone complement the 8-m resolution DEM from DEMNAS and enabled us to precisely locate the fault and enhanced our ability to identify small-scale scarps and associated displacements. The fault is primarily visible through linear topographic landforms (scarps), including those that offset river channels consistently. The data allowed us to trace the fault, and the mapping results are presented in Figs. 2–12.

During our field reconnaissance, we checked the fault trace wherever we could recognize it on the DEMs. Some of the fault traces were visible in the bedrock. We used the location where this fault was exposed in the bedrock as a reference point to project the fault into the loose Quaternary sediment unit, which presents a greater challenge for fault detection.

The Aceh Fault is characterized by prominent right-lateral displacements of channels and ridges, with cumulative offsets typically ranging from several tens to hundreds of meters. In contrast, only a limited number of locations exhibit measurable offsets at the meter scale. This contrast is likely due to the climatic condition favouring strong erosion (Reitman et al., 2023). These geomorphic features are interpreted as the result of repeated seismic events along localized fault planes, forming cumulative offsets. Detailed documentation and quantitative measurements of these offsets have been provided in previous studies (e.g., Marliyani et al., 2023), offering insight into the fault's long-term slip behavior.

While cumulative offsets along much of the Aceh Fault reflect repeated seismic activity, the fault's southeastern terminus presents a more complex geomorphic expression. Near its junction with the Tripa Fault, the fault trace is marked by a narrow canyon bordered by steep topography. In this area, the fault exhibits a right bend, forming a pressure ridge that structurally separates the Aceh and Tripa Faults (Fig. 3). A narrow linear valley follows the main trace of the Aceh Fault and captures most of the drainage from the surrounding hillslopes, complicating the identification of lateral displacements along this section. However, a secondary fault strand offsets several channels with apparent right-lateral displacements, indicating localized deformation and active faulting (Fig. 3).

Further northwest, in the central section of the Aceh Fault, near its

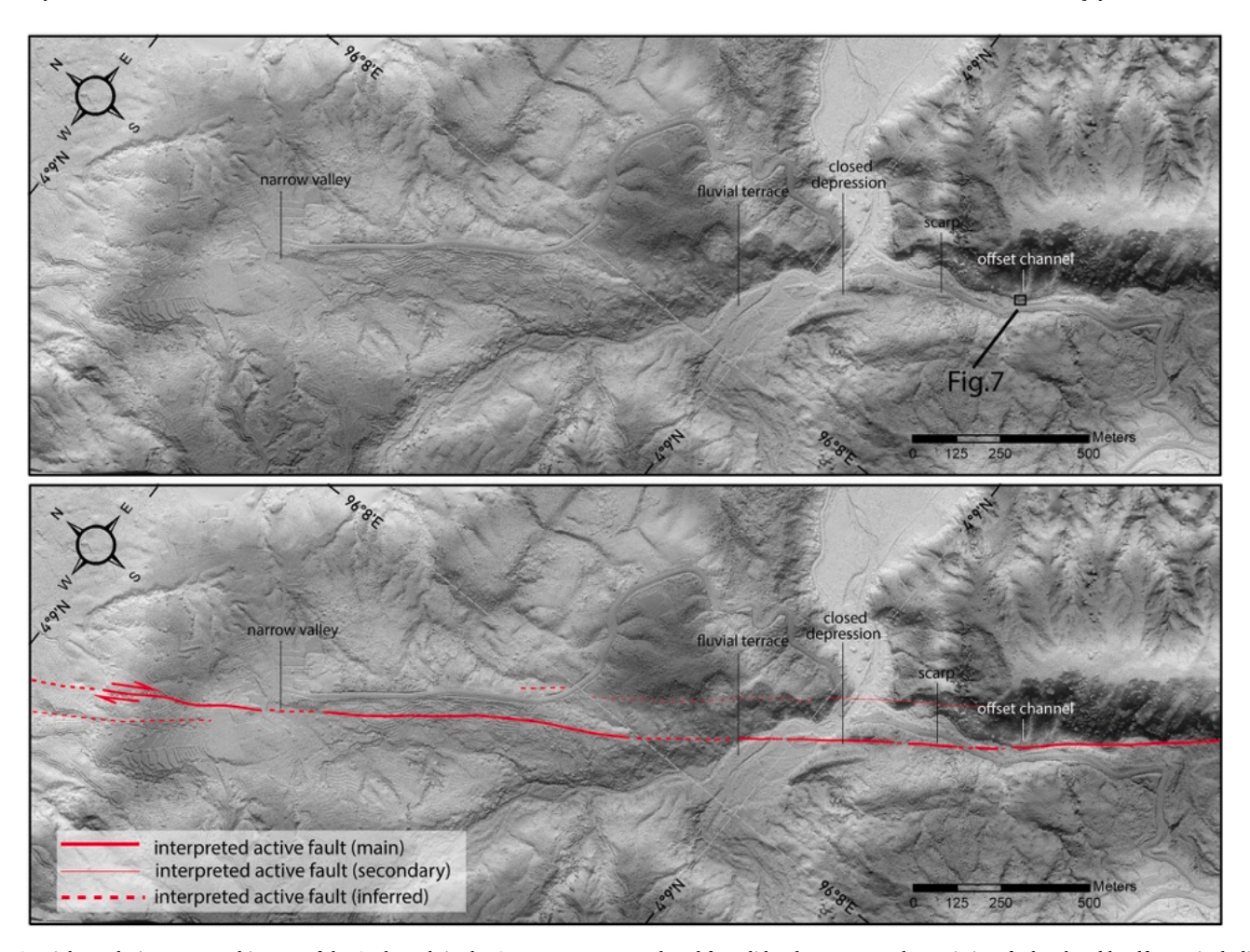


Fig. 6. High-resolution geomorphic map of the Aceh Fault in the Geumpang area, produced from lidar drone survey data. Distinct fault-related landforms, including displaced stream channels and terrace offsets, help delineate the active fault trace. See Fig. 5 for site context.

intersection with the Batee Fault, the fault zone is defined by a narrow, linear canyon incised into steep mountainous terrain. The adjacent ridges rise up to 600 m above the valley floor (Fig. 4). Within this section, multiple fluvial channels display separations on the order of several hundred of meters. Most of these channels flow perpendicular to the fault trace, and some show well-developed shutter ridge morphologies. These characteristics provide abundant piercing points, making this area highly suitable for slip-rate estimation. Nevertheless, the remoteness and inaccessibility of this region—characterized by the absence of established roads and dense primary forest—currently hinder direct field investigations.

In the Geumpang area, the fault continues northwestward through a rugged mountain belt before entering a 3.8 km-wide linear valley bounded by the fault zone. This geomorphic configuration facilitates the development of transverse channels draining from the uplifted southwestern block toward the northeastern block. Multiple offset channels have been identified in this region, with displacements ranging from 12.6 to 323 m. The fault here dissects Quaternary alluvial deposits and various levels of fluvial terraces (Figs. 5-9), offering significant potential for paleoseismic investigation and long-term fault slip analysis. Through detailed field mapping, we identified several previously undocumented geomorphic features near Geumpang village, including the fault displacing a ridge and adjacent gully (Fig. 7). This observation allowed for a more precise delineation of the active fault strand in this area. The observed offset at this site is approximately 6 m, which may correspond to surface rupture from one or more recent earthquakes along this section of the fault.

Following the fault trace northwestward into the Mane area, the Aceh Fault traverses mountainous terrain before entering a narrow valley approximately 1.3 km in width. Along this section, we observed a suite of tectonic geomorphic features including fault scarps, offset channels, and pressure ridges. Measurable channel displacements range from several tens to hundreds of meters. Notably, the fault bifurcates in this area, with one branch forming the Seulimeum Fault (Fig. 10).

Continuing further northwest into the Jantho area, the fault cuts through terrain with elevation between approximately 300 and 800 m above sea level. This section is characterized by minor structural complexities, including both right- and left-stepping fault sections (stepovers) ranging from 0.2 to 2 km in width, as well as multiple fault branches.

In the northwesternmost section of the fault in the Indrapuri region, there is a prominent morphological break characterized by a vast alluvial plain adjacent to a high mountainous region, both bounded by the fault into southwestern and northeastern blocks, and occurring at a markedly larger scale than the previous section. The southwestern block is composed of Jurassic argillaceous and siliceous limestone of the Barisan Range while the northeastern block consists of a broad alluvial plain (Fig. 2). The elevation difference between the two blocks is approximately 1200 m. However, the active fault trace within the alluvial plain is not readily identifiable, likely due to sediment cover and lack of clear surface expression. Importantly, this $\sim\!1200\text{-m}$ topographic break does not reflect vertical displacement associated with recent fault movement, but rather represents a long-term lateral offset of the Barisan Range, resulting from earlier orogenic processes. Regional geologic

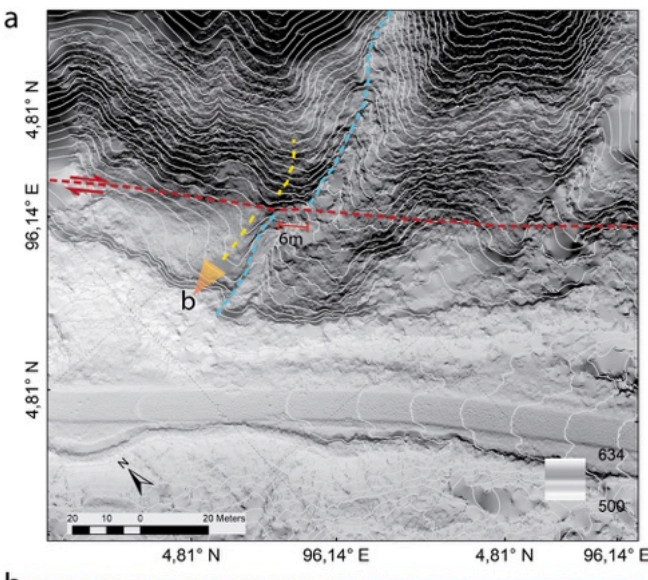




Fig. 7. Field-based observations of faulted landforms in the Geumpang area. The small triangle marks the viewing direction of the photograph shown in panel (b). The Sumatran Fault is highlighted by the bold dashed red line, which offsets both a local ridge (outlined in yellow) and a nearby gully (blue dashed line marking the thalweg). The location of this image corresponds to the area shown in Fig. 6. (For interpretation of the references to colour in this figure legend, the reader is referred to the web version of this article.)

mapping by Bennett et al. (1981) indicates a lateral displacement of approximately 20 km of the Oligocene Meucampli Formation across the fault in this region.

Analysis of offshore bathymetric data reveals a distinct linear morphological break trending northwest of Pulo Aceh, aligned with the onshore trace of the Aceh Fault. This feature consists of a narrow, elongated depression flanked by subtle scarps, which is consistent with the expected geomorphic expression of a strike-slip fault segment in a submarine setting. Based on this alignment and continuity of geomorphic indicators, we interpret this structure as a northwestward offshore continuation of the Aceh Fault, extending its length by approximately 60 km beyond Pulo Aceh. This extension significantly increases the total fault length, thereby raising its potential maximum earthquake magnitude and emphasizing its importance in regional seismic hazard assessments.

4.2. Paleoseismic trenching results

We carefully selected the paleoseismic trenching site after evaluating several potential locations based on critical criteria, including fault exposure, sediment accumulation, stratigraphic clarity, and the availability of datable organic materials. The chosen site is located in Geumpang Village, within the Mane sub-regency of Aceh Province (Figs. 2, 8, and 13). At this location, we excavated two trenches (T1 and T2) to investigate surface-rupturing earthquake events and to reconstruct the recent rupture history of the Aceh Fault.

4.2.1. Site morphological setting

As noted earlier, northern Sumatra is characterized by very dense vegetation where it is almost impossible to penetrate. Where it is not forested, the land is usually heavily modified, which strongly impacts the morphology and can make recognition of landform associated with fault activity more difficult. The trench site we selected is characterized primarily by a well-defined linear fault scarp that is unambiguously related to tectonic activity, with no evident human modification. Evidence for that scarp can be traced laterally for several hundreds of meters, although it is mostly discontinuous. The scarp appears as a prominent topographic break approximately 6 m high, with the southwestern side up, which trends northwest-southeast (Fig. 13). The downthrown part is swampy, suggesting that the fault controls both topography and surface hydrology. The scarp lies roughly 0.5 km northeast of the mountain front of the Bukit Barisan Range. Although it could not be totally ruled out that in the past a part of this scarp was acting as a river riser, the current local drainages do not support this interpretation. Conversely, the detailed topography of the site reveals that the scarp topography is not completely uniform. The scarp topography is rather characterized by two small eminences separated by a small subdued saddle that lies about 1.5 m below the top of the scarp. Although it is clear that a lot of the current topography results from human modifications and thus, it calls for caution when one conducts geomorphological interpretation, in view of the local topography (Figs. 8 and 13) we suggest that this saddle corresponds to the ancient thalweg of a gully that was flowing northward from the Bukit Barisan Range mountain front, toward the centre of the valley. The fault motion locally impeded the gully from flowing across the scarp, causing the river to be progressively deflected eastward to its present course (Fig. 8). While an apparent vertical offset is visible in the topography, this could also reflect lateral translation of pre-existing relief rather than true dipslip displacement. The geomorphic configuration of the saddle suggests that it may act as a natural trap for fluvial deposits. Hence, this saddle bears good potential for river sediments to contrast with the highly weathered volcanic breccia that has altered into a whitish-colored clay unit and forms most of the basement units in this area. These river sediments could provide well-stratified deposits with abundant organic materials, making it highly suitable for stratigraphic and radiocarbon dating analyses.

4.2.2. Stratigraphy

Trenching at the site exposed the Aceh Fault displacing a heavily weathered profile of the volcanic breccia unit. This unit is juxtaposed in fault contact with fluvial channel deposits that are themselves affected by fault. Hence, the overall stratigraphic sequence observed at the trench site consists of a basal weathered volcanic breccia unit, which forms the bedrock, overlain by sandy gravel units derived from fluvial processes sourced from the Bukit Barisan Range (visible only in Trench 1), channel fills within the fault-generated trough at the base of the scarp, and organic-rich swamp deposits forming the uppermost layers of the section (Figs. 14–16).

Within this stratigraphy, multiple distinct infilling episodes can be recognized that have undergone fault-related deformation, such as folding and tilting. The channel fills contain wood and charcoal fragments, while the overlying swamp deposits are notably rich in organic material. The swampy environment has preserved these organic components well, with many layers containing abundant, well-preserved wood fragments. The preservation of wood and charcoal fragments within the channel fills and swamp deposits is likely due to the anoxic

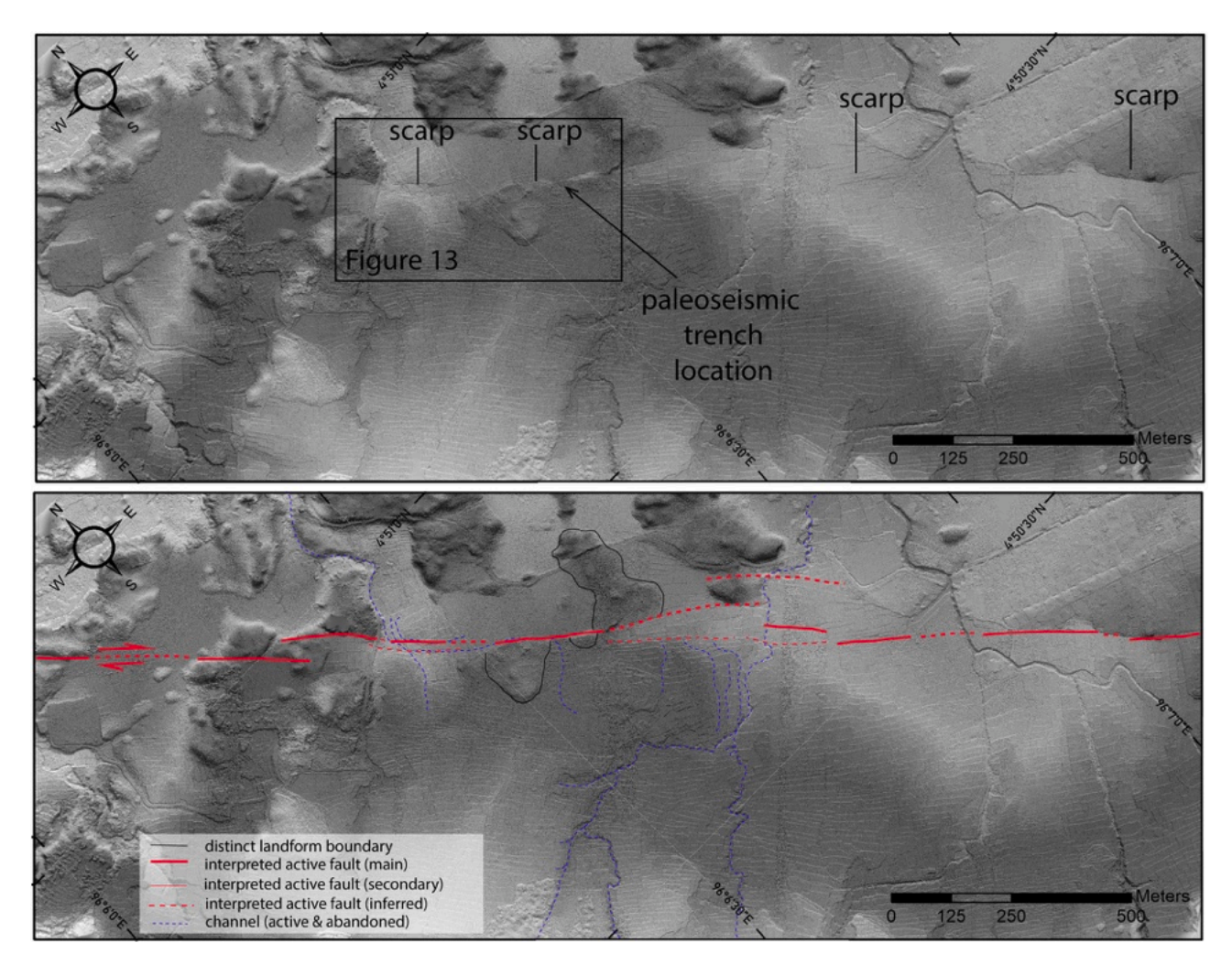


Fig. 8. Map showing the interpreted active fault, identified by observing tectonic geomorphic features such as scarps, offset channels, offsetting fluvial terraces of the Aceh Fault near Geumpang village. The hillshaded Digital Elevation Model (DEM) used as the basemap is from our lidar drone survey. See Fig. 5 for reference to location.

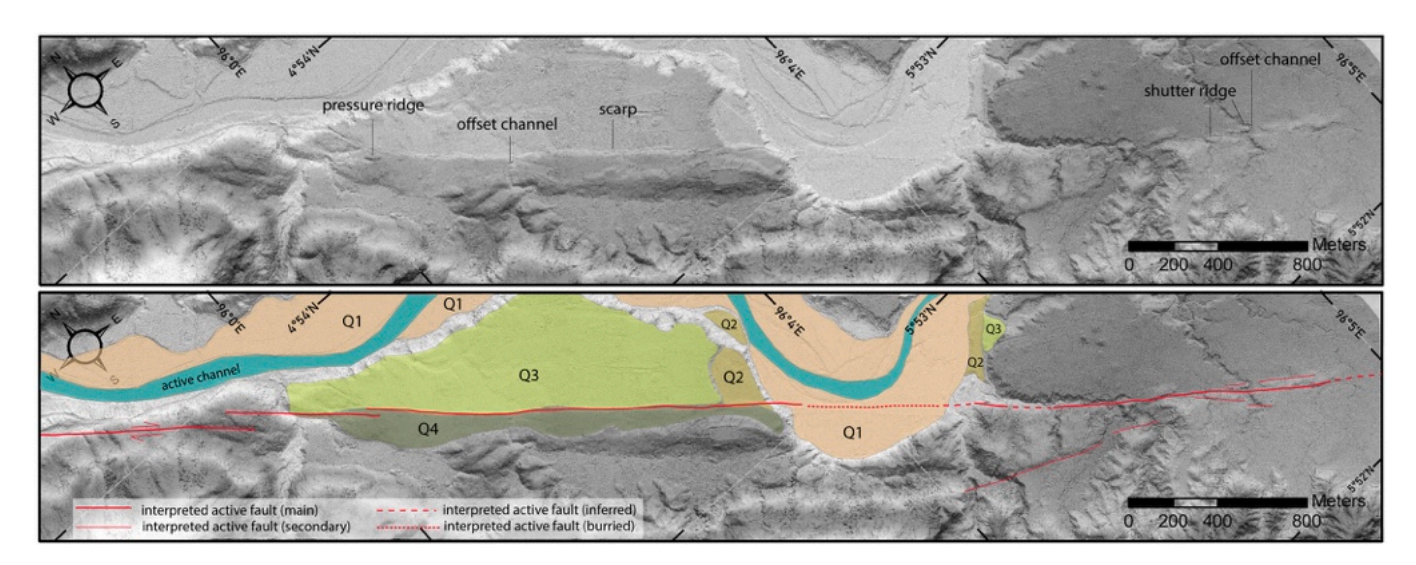


Fig. 9. Detailed map of the Aceh Fault segment in Geumpang based on lidar topography, revealing key geomorphic features such as fault scarps and offset fluvial elements. This figure complements Fig. 8 by emphasizing geomorphic continuity and structural interpretation across the trench site. See Fig. 5 for reference to location.

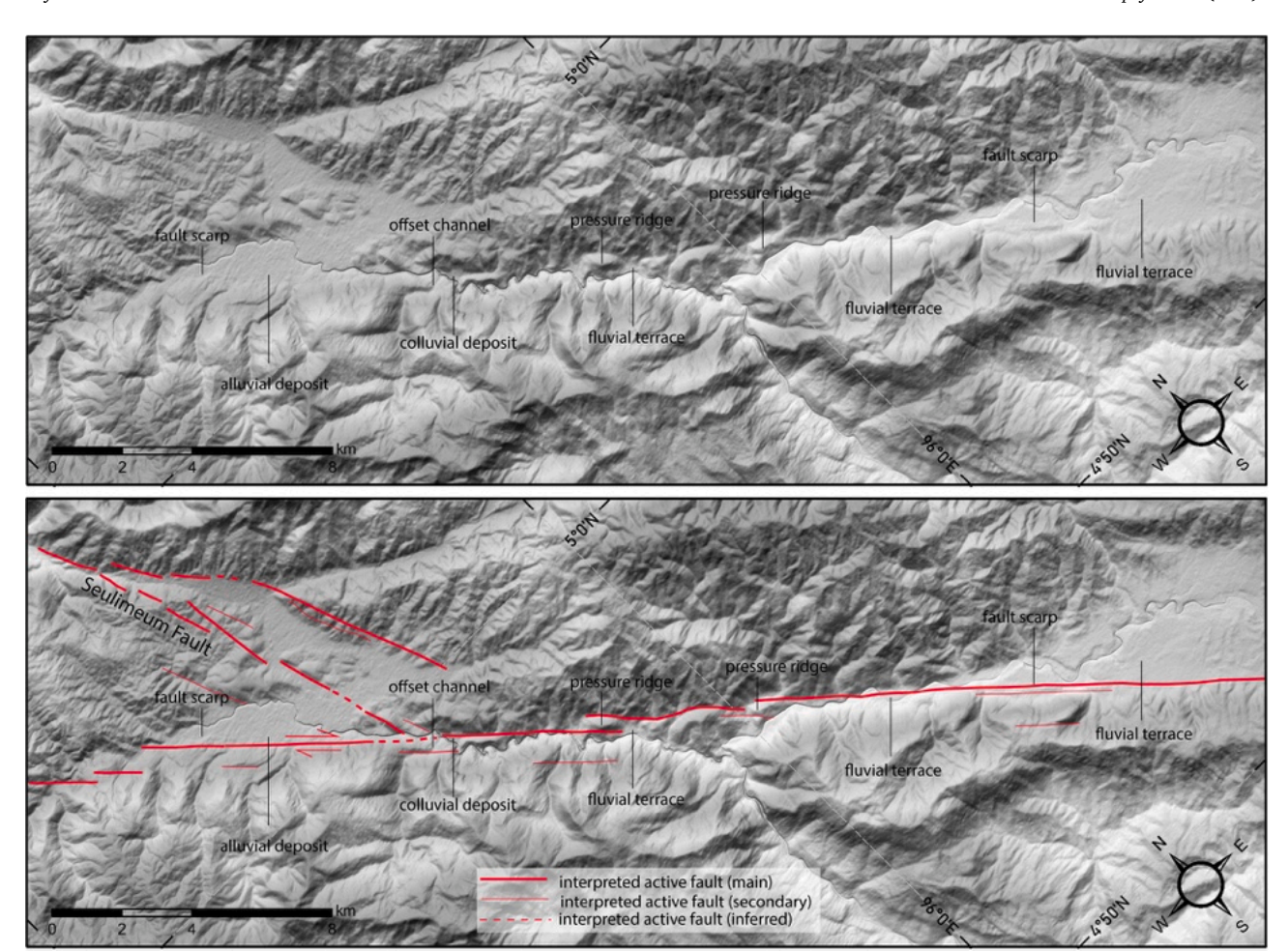


Fig. 10. Interpreted fault trace of the Aceh Fault in its northeastern extent near the junction with the Seulimeum Fault. Geomorphic indicators include pressure ridges and deflected stream networks. The shaded terrain basemap is generated from DEMNAS (https://tanahair.indonesia.go.id/demnas/#/). Regional context is shown in Fig. 2.

conditions typical of waterlogged environments. In such settings, the lack of oxygen inhibits the activity of decay organisms, particularly fungi, which require oxygen to metabolize the chemical constituents of wood. As a result, organic materials like wood can remain remarkably intact for extended periods (Pedersen et al., 2012).

The uppermost 25 cm of our section were not considered in the further analyses of our trenches as they are heavily disturbed by human and animal activities. This disturbed layer was removed during trench preparation to stabilize the wall and is therefore not shown in the stratigraphic logs. When preserved in photographs, it is clearly identifiable as a modified surface horizon and lies above Unit 100, which marks the top of the analyzed stratigraphy. Although the volcanic breccia unit is significantly weathered at the trench site, observation of the similar formation at a nearby location where this unit is relatively unweathered indicates that the unit occasionally contains burned wood. In our trench, several instances of charred wood were found within the weathered clay derived from the breccia, which were sampled for 14C dating. Two wood samples (KNG-22 and KNG-19) yielded calibrated radiocarbon ages of 17,588 \pm 60 BCE and 17,765 \pm 135 BCE, respectively (Fig. 14), indicating that they are significantly older than the overlying stratigraphy.

We observed an accumulation of large boulders near the scarp in Trench 2. This concentration is interpreted as the result of gravity-driven colluvial transport and localized deposition within the fault-bounded trough, possibly augmented by short-distance fluvial reworking during high-energy flow events. The scarp likely acted as a natural sediment trap, facilitating the preferential concentration of coarse material in this

area

A summary of all stratigraphic units identified in both trenches is provided in Fig. 17, including unit descriptions, relative stratigraphic positions, and corresponding radiocarbon dates. Unit numbers increase with age, from unit 100 (youngest) to units 830–800 (oldest). The heavily weathered volcanic breccia, forming the clay-rich unit at the base of the trench, is considered the oldest lithologic component. While lateral age differences across the fault cannot be resolved, the volcanic breccia units are treated as a single, regionally extensive unit predating the overlying depositional sequence.

4.2.3. Observation of faulting

Clear evidence of faulting is observed in both trenches, particularly in Trench 1. The main fault is expressed as a steep, near-vertical discontinuity, most visible through the offset and truncation of unit 800—the weathered clay derived from volcanic breccia (Fig. 14). The principal fault zone is relatively narrow, less than 0.5 m in width, and is accompanied by minor normal faulting and sediment-filled fissures.

In Trench 2, the fault expression is more subdued (Fig. 16). The absence of fluvial deposits, which serve as excellent stratigraphic markers in T1, makes fault interpretation more challenging. However, the fault is inferred from the offset in the weathering profile of the volcanic breccia unit, which is in contact with the organic-rich swamp deposits. These deposits are stratigraphically equivalent to the channel fills and swamp sediments documented in Trench 1.

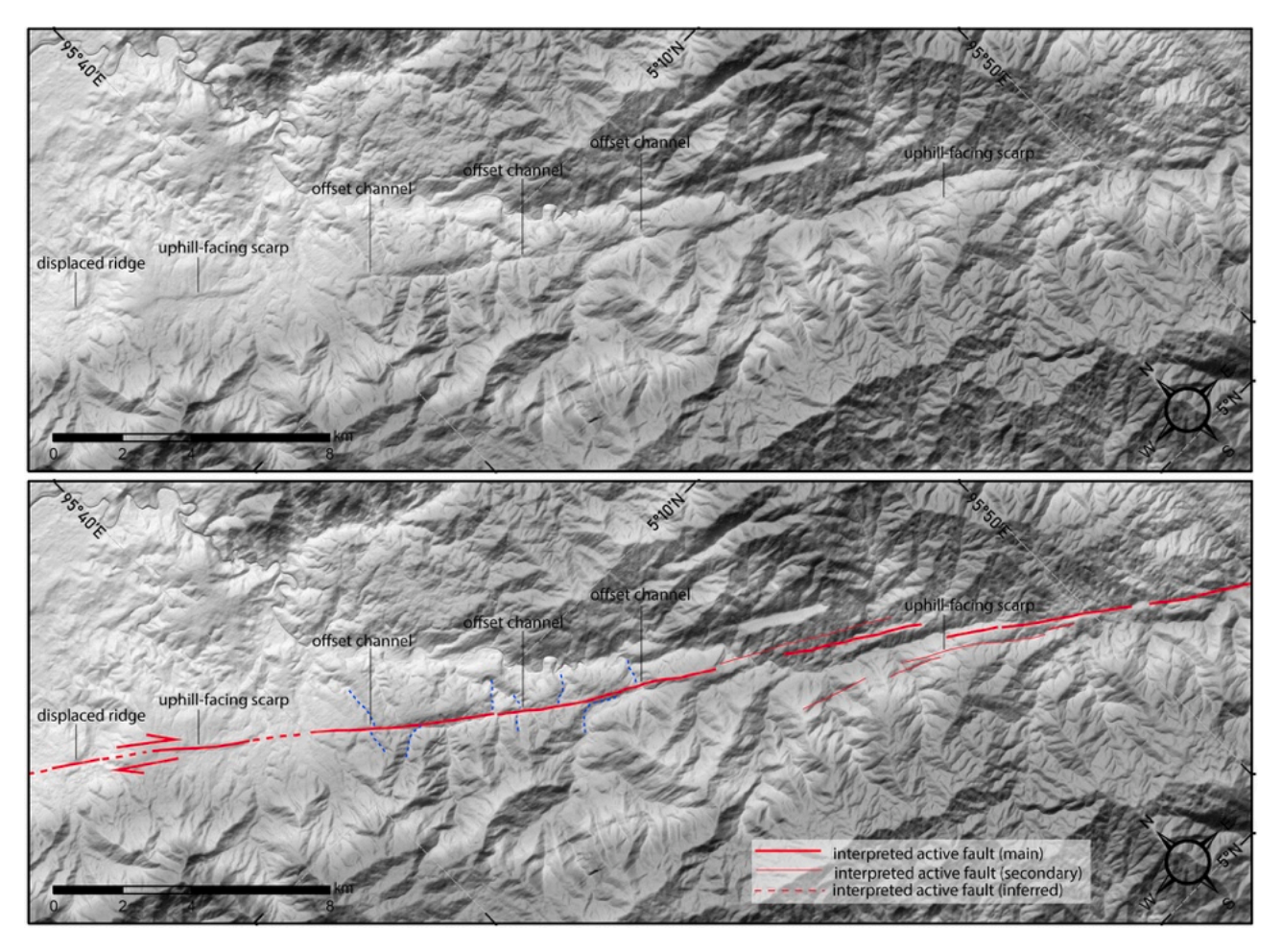


Fig. 11. Active fault interpretation along the central Aceh Fault, highlighting geomorphic markers such as offset drainages (blue dashed lines) and pressure ridges. Hillshade rendering is derived from 8-m DEMNAS data (https://tanahair.indonesia.go.id/demnas/#/). The fault alignment is informed by geomorphic and structural correlations. See Fig. 2 for broader location. (For interpretation of the references to colour in this figure legend, the reader is referred to the web version of this article.)

4.2.4. Event identification and chronology

4.2.4.1. Rupture evidence observed in trenches. Evidence for surface-rupturing paleoearthquakes in Trenches 1 and 2 is revealed through

cross-cutting relationships between fractures and sedimentary units, as well as the sedimentological characteristics and provenance of deposits. The primary indicators of faulting include displaced and truncated strata, folding near the fault zone, the presence of colluvial wedges, and

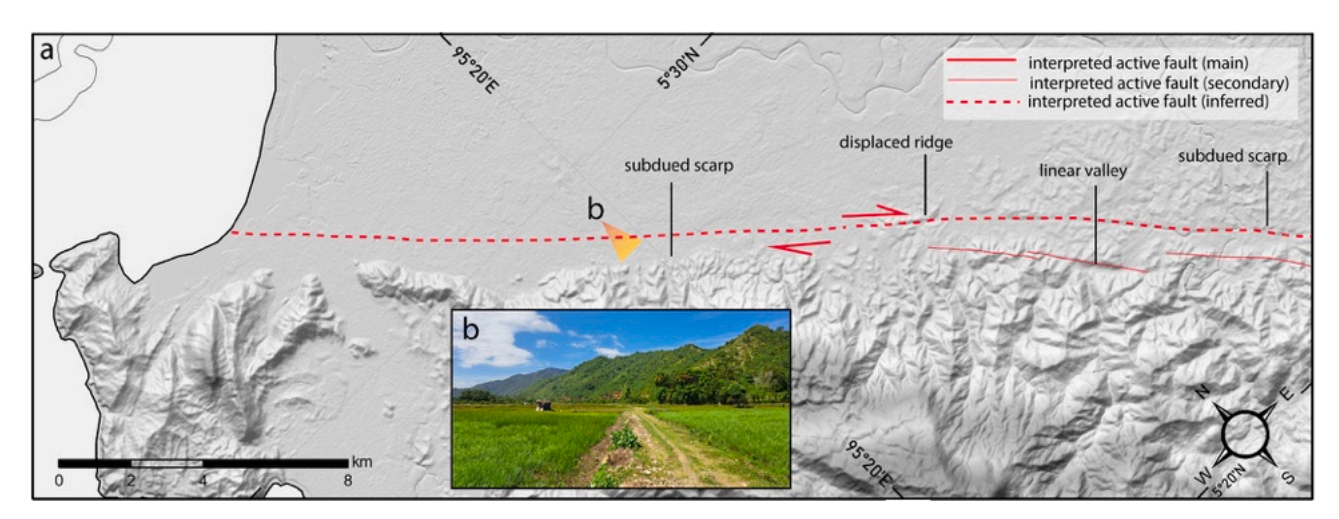


Fig. 12. Geomorphic expression of the Aceh Fault through Banda Aceh city. Despite urban development, subtle features such as linear alignments and subdued scarps mark the fault trace. The small triangle marks the viewing direction of the photograph shown in inset figure (b). Hillshaded relief from DEMNAS (https://tanahair.indonesia.go.id/demnas/#/) is used to enhance visualization. See Fig. 2 for spatial reference.

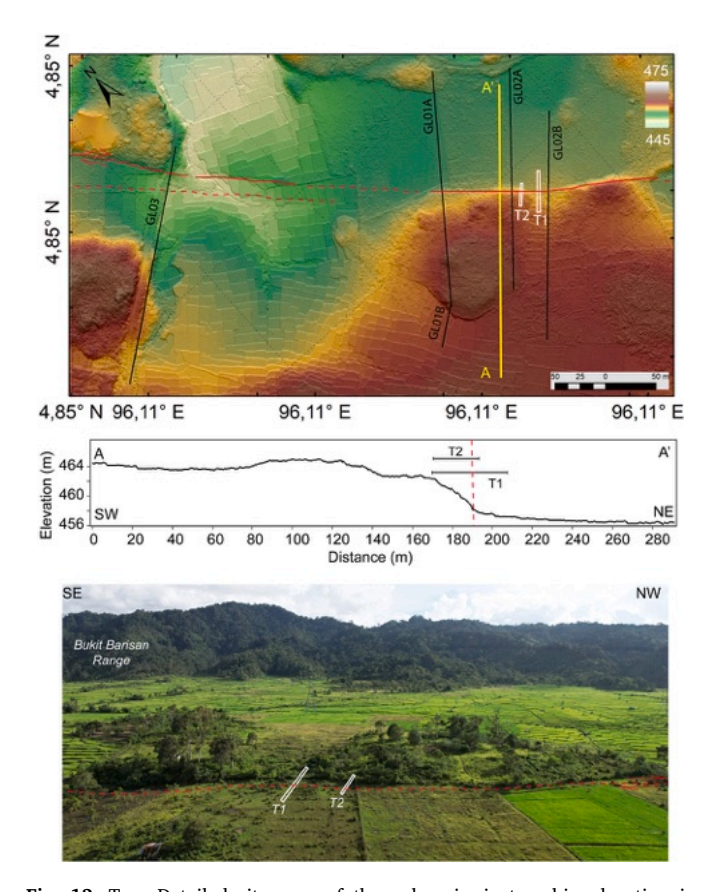


Fig. 13. Top: Detailed site map of the paleoseismic trenching location in Geumpang Village, Mane sub-regency. Trench T1 and T2 locations are shown in white polygons; black lines represent resistivity survey transects. Middle: Topographic profile along line A–A', showing a \sim 6-m-high scarp interpreted as the fault trace (marked by a dashed red line). Bottom: Oblique drone photograph providing a visual overview of the study area, with fault-displaced terrain and trench locations annotated. See Fig. 8 for location context. (For interpretation of the references to colour in this figure legend, the reader is referred to the web version of this article.)

upward drag of sedimentary layers along fault planes (Table 1).

In the northeastern part of Trench 1, vertical separation of the basement unit (Unit 800) at m23.5 that may result from either lateral translation or a minor dip-slip component, created accommodation space for the overlying deposition of Units 700, 600, and 500 (Fig. 18). Although specific fault planes cannot be definitively attributed to this early deformation, the stratigraphic configuration and sediment infill suggest activity along the main fault zone at the northeastern end of the trench. The observed trough reflects an erosional channel formed by vigorous fluvial processes, consistent with the presence of coarse boulder deposits. Higher in the section, Unit 500 and 400 are cut by a visible fracture, interpreted as direct evidence of a subsequent surfacerupturing event. The bounding contacts of Units 700 to 500 adjacent to the fracture show deformation consistent with displacement along the fault zone, although the exact sense of movement (upward, downward, or lateral mismatch) cannot be uniquely determined from the exposure. This deformation likely records reactivation of the fault zone during a later event.

Additional rupture evidence is observed in Trench 2, where a fracture offsets Unit 650 and is capped by Unit 305. This structure likely corresponds to the same rupture phase that affected Unit 500 in Trench 1 (E3). We should note, however, the upper termination of this fault strand shows minimal vertical separation and is weakly expressed in the stratigraphy. Because most of the fault continues upward into younger units, this feature is not considered reliable evidence for a separate earlier event (E3) and is therefore classified as undifferentiated.

Following this event, fluvial processes eroded and deposited channel and overbank sediments (Units 336 to 310), followed by the accumulation of colluvial Unit 300. The stratigraphic sequence in Trench 2 is capped by Unit 200, an organic-rich gravel and sand layer that is gently warped near the fault trace. This unit is in turn overlain by Unit 100, a disturbed surface horizon. More detailed interpretation of the deformation and its relation to the timing of faulting is presented in the following section.

4.2.4.2. Paleoseismic event interpretation. Based on the structural and stratigraphic observations described above, we interpret evidence for three discrete surface-rupturing paleoearthquake events at the site. The earliest event, designated as Event E3, is primarily inferred from the

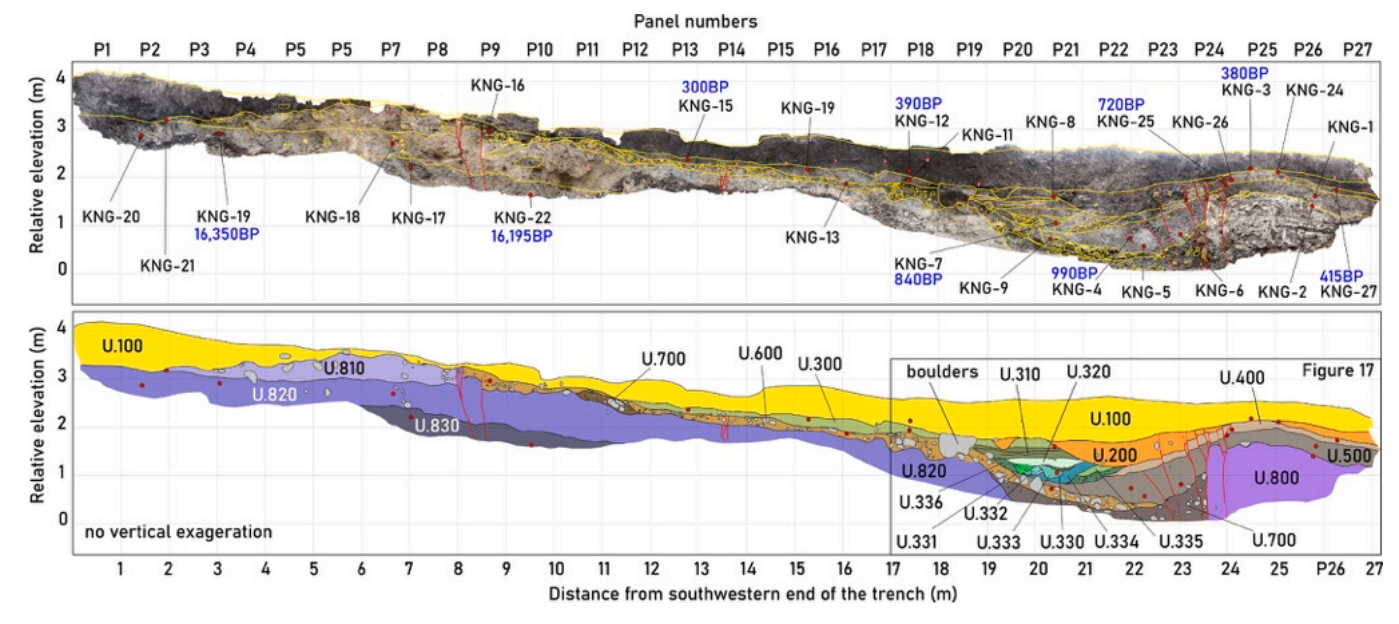


Fig. 14. Composite image of Trench 1 (T1), showing both a photomosaic (top) and interpretive photolog (bottom). Stratigraphy is colour-coded by unit, increasing in number with age. Faults are marked in red, while yellow and black lines trace key stratigraphic boundaries. Radiocarbon sampling locations are indicated with red dots. (For interpretation of the references to colour in this figure legend, the reader is referred to the web version of this article.)

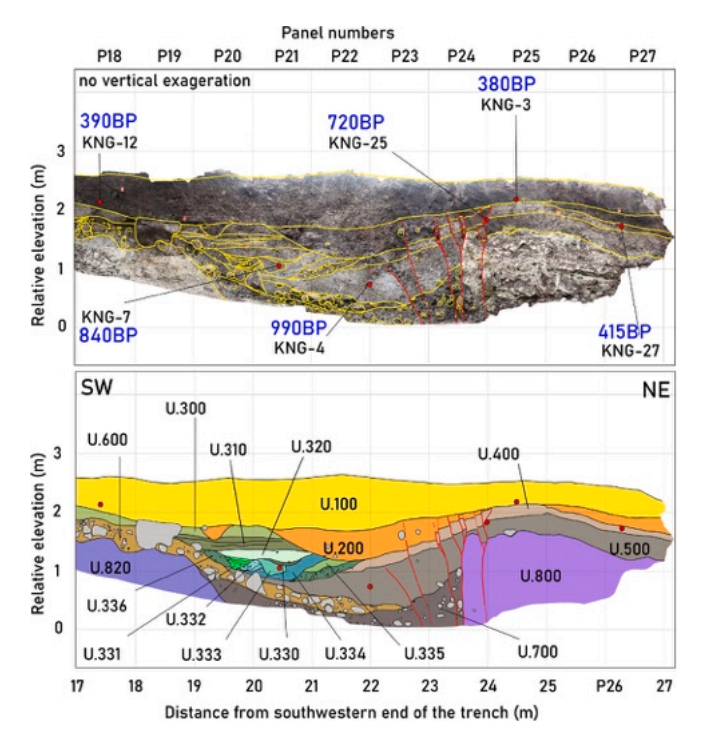


Fig. 15. Close-up view of Trench 1 highlighting detailed deformation features within the upper 2 m of stratigraphy. The photomosaic (top) and photolog (bottom) illustrate tilted and offset sediment layers across the fault. Key horizons and faults are mapped, with sample locations marked.

presence of stratigraphic accommodation space that enabled the deposition of Units 700, 600, 500, and 400. While no fault can unambiguously be tied to this event, the observed offset of the basement and the geometry of overlying units suggest that faulting must have preceded their deposition. This event is therefore tentatively associated with movement along the northeastern segment of the main fault zone.

Event E2 is supported by direct evidence: a fracture that offsets Units 400 and 500 in Trench 1, and a fault in Trench 2 that displaces Unit 650 and is sealed by Unit 350. Additionally, deformation affecting Units 700 to 500 (T1) suggests displacement across the fault zone during this event. While the original geometry appeared consistent with upward warping, we acknowledge that this could equally reflect lateral translation across nonplanar units, producing apparent offset without a definitive vertical component. Event E2 occurred before the accumulation of Units 336 through 310 (T1). The stratigraphic record also indicates post-event fluvial incision and deposition, followed by colluvial accumulation (Unit 300) along the fault scarp. The fault strand terminating in U500 and capped by U400 in Panel 22-23 (Figs. 14 and 17) is interpreted as weak evidence for E2, consistent with faulting after U500 deposition. However, the small vertical separation and absence of surface rupture mean that the structure could also reflect slip during E1 that did not reach the ground surface. Such incomplete rupture propagation is consistent with other trench studies showing upward terminations that stop below the ground surface (Bonilla and Lienkaemper, 1991). In Trench 2, two fault strands juxtapose bedded U810 against massive U800 (Fig. 16), indicating lateral translation after U550 deposition and prior to U340. This geometry, combined with the stratigraphic offset, provides strong structural evidence for E2. At T1 (Panel 22–24, Figs. 14, 15), three fault strands cut through the fault zone. Of these, only the main strand that displaces U800 and overlying units shows clear structural evidence consistent with E2 movement. The other two strands

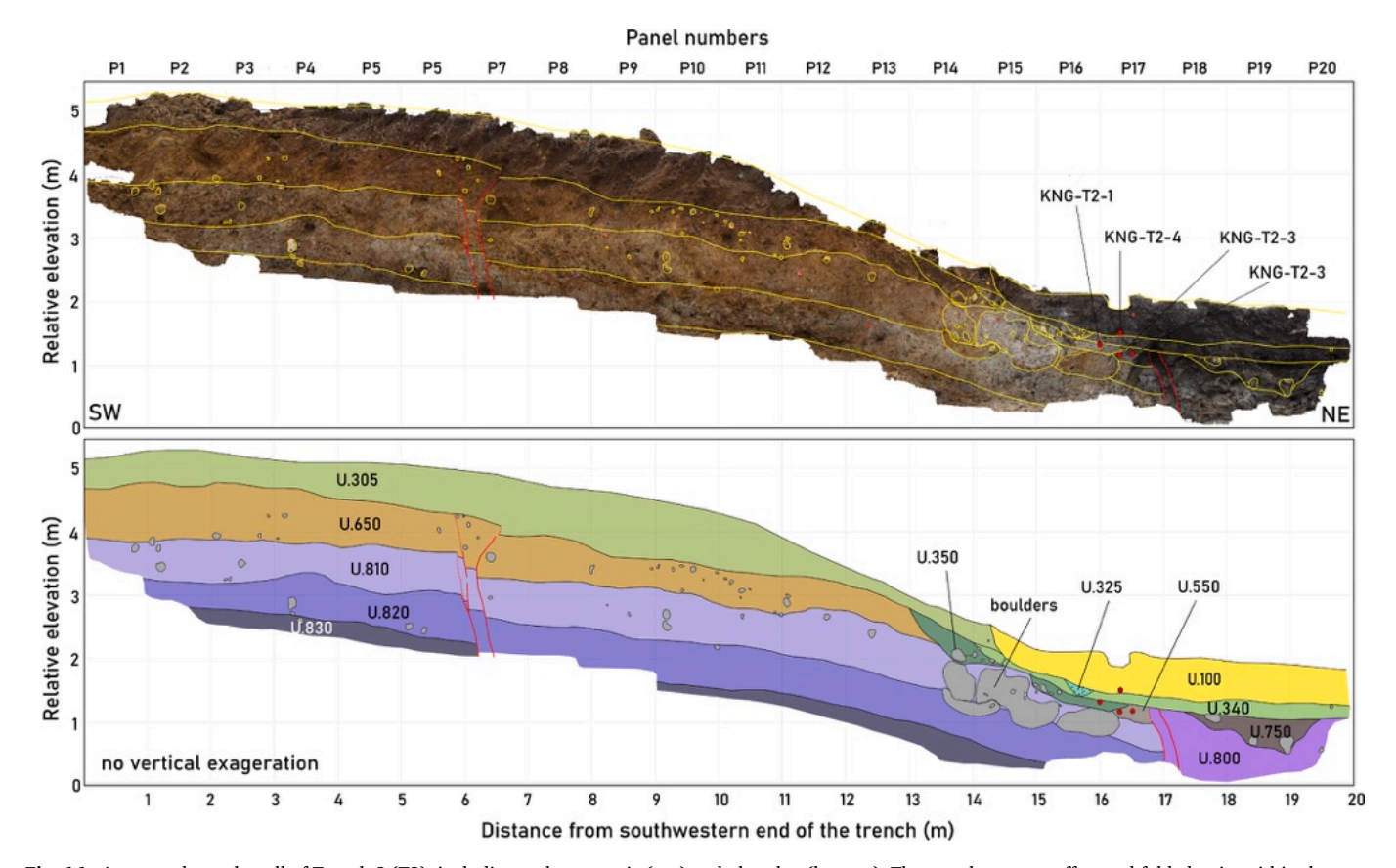


Fig. 16. Annotated trench wall of Trench 2 (T2), including a photomosaic (top) and photolog (bottom). The trench exposes offset and folded units within the upper sedimentary sequence. Structural and stratigraphic contacts are indicated, along with radiocarbon sample sites (red dots). (For interpretation of the references to colour in this figure legend, the reader is referred to the web version of this article.)

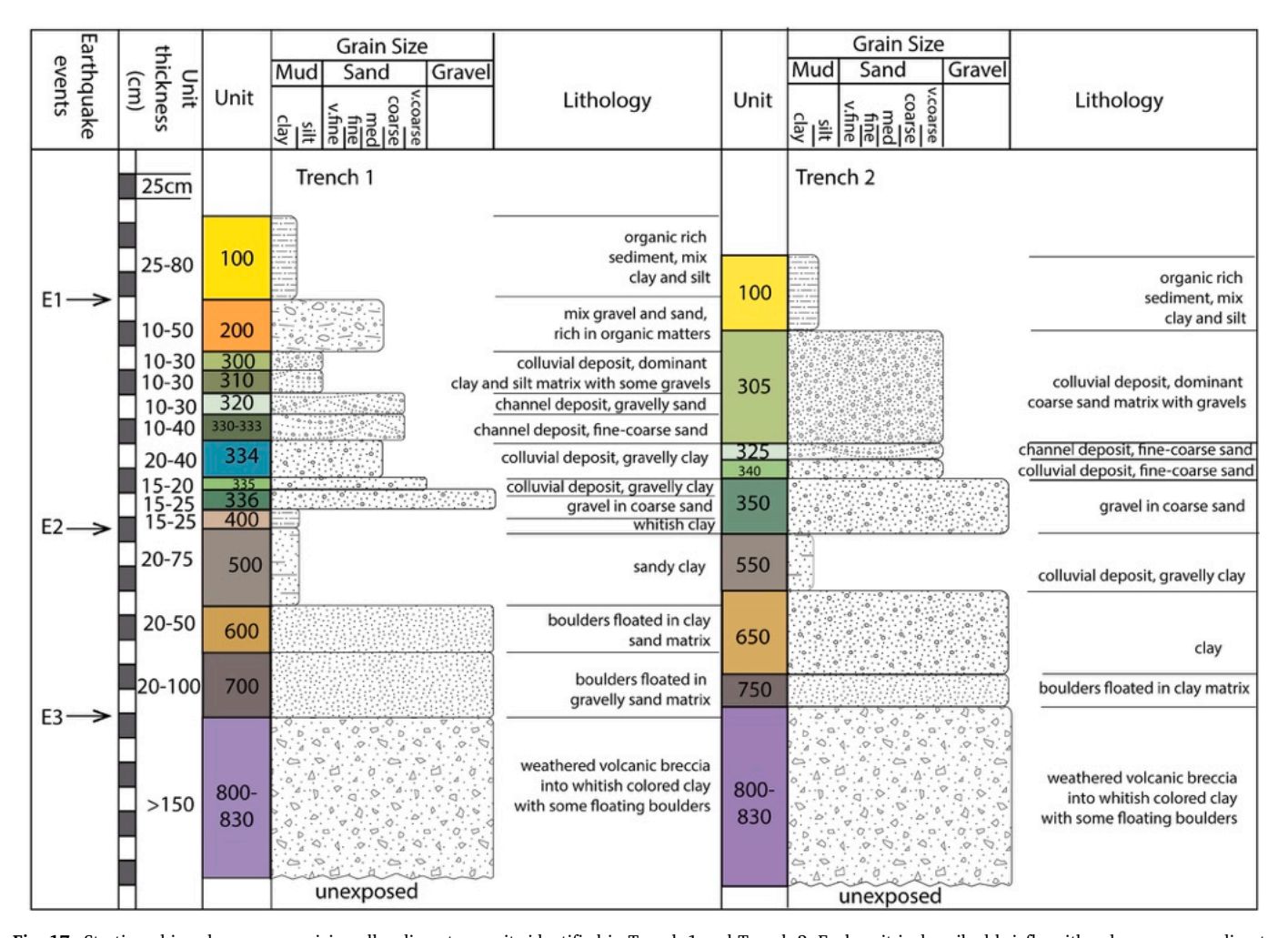


Fig. 17. Stratigraphic column summarizing all sedimentary units identified in Trench 1 and Trench 2. Each unit is described briefly with colors corresponding to those used in the trench logs (Figs. 14–16). Radiocarbon dating results and unit relative ages are incorporated.

exhibit nearly constant vertical separation with depth, suggesting they may not have moved significantly during E2 and may represent earlier faulting episodes or inactive structures at the time of this rupture. This revised interpretation reflects the likelihood that E2 slip was localized on a subset of fault strands, rather than distributed equally across the entire fault zone.

The most recent event (E1) is recorded by multiple fault strands that offset the base of Unit 200 but do not affect its top, along with localized folding of Unit 200 on the upthrown block near the fault zone. Unit 200

was deposited within a trough-shaped depression, which explains its nonplanar base and the horizontal geometry of Unit 300 beneath it on the downthrown side. In contrast, the overlying Unit 100 is not deformed, bracketing the most recent rupture between the deposition of these two units. Folding of Unit 400 is attributed to an earlier event (E2), after which Unit 200 onlapped the uplifted structure. Subsequent folding during E1 is superimposed on this earlier geometry. The relatively flat Unit 100–200 contact partly reflects modern surface modification, which may obscure subtle post-depositional deformation.

Table 1Summary of event evidence for ground-rupturing earthquakes exposed in Trench 1 and Trench 2.

Events	Units	Exposure	Evidence
E1	Top of unit 200 (T1), bottom of unit 100	Panel 22, 23, 24 ^a	Fault that broke the uppermost of unit 200, upper termination of faults at the bottom of unit 100
E2	Top of unit 400 (T1)	Panel 8, 9, 14, 22, 23, 24 Panel 17 (T2)	Fault that broke the uppermost of unit 400 at T1. Fault that broke unit 550 and upper terminated at the bottom of Unit 340 at T2. Juxtaposition of U810 and U800 in T2 indicate lateral translation post-U550 and capped by U340 making it strong evidence for E2
			Fault strand terminates at base of U600 (debris-flow deposit) at Panel 8–9 of T1 likely postdates U600 deposition (attribute to E2 or E1). Some uncertainty remains due to erosional upper contact. Fault that offsets U820 and U600 in panel 14 of T1 capped by erosional surface at base of U300. The event attribution is uncertain (E2 or E3). The weak constraint is due to poor exposure.
E3	Top of unit 600, bottom of unit 300 (T1)	Panel 8, 9, 14, 24 (T1) Panel 6, 7 (T2)	Upper termination of faults at the bottom of unit 300 at T1 Fault that broke unit 650 at T2. The fault has minimal vertical separation; upper termination weak and fault continues higher. Classified as weak evidence for E3. Fault in panel 8–9 offsets Units 810 and 600 and capped by U100 is a result of indifferentiated faulting (E3–E1). The
			timing cannot be resolved due to erosional truncation and lack of overlying stratigraphy.

^a Panel numbers correspond to photologs in Figs. 14-16.

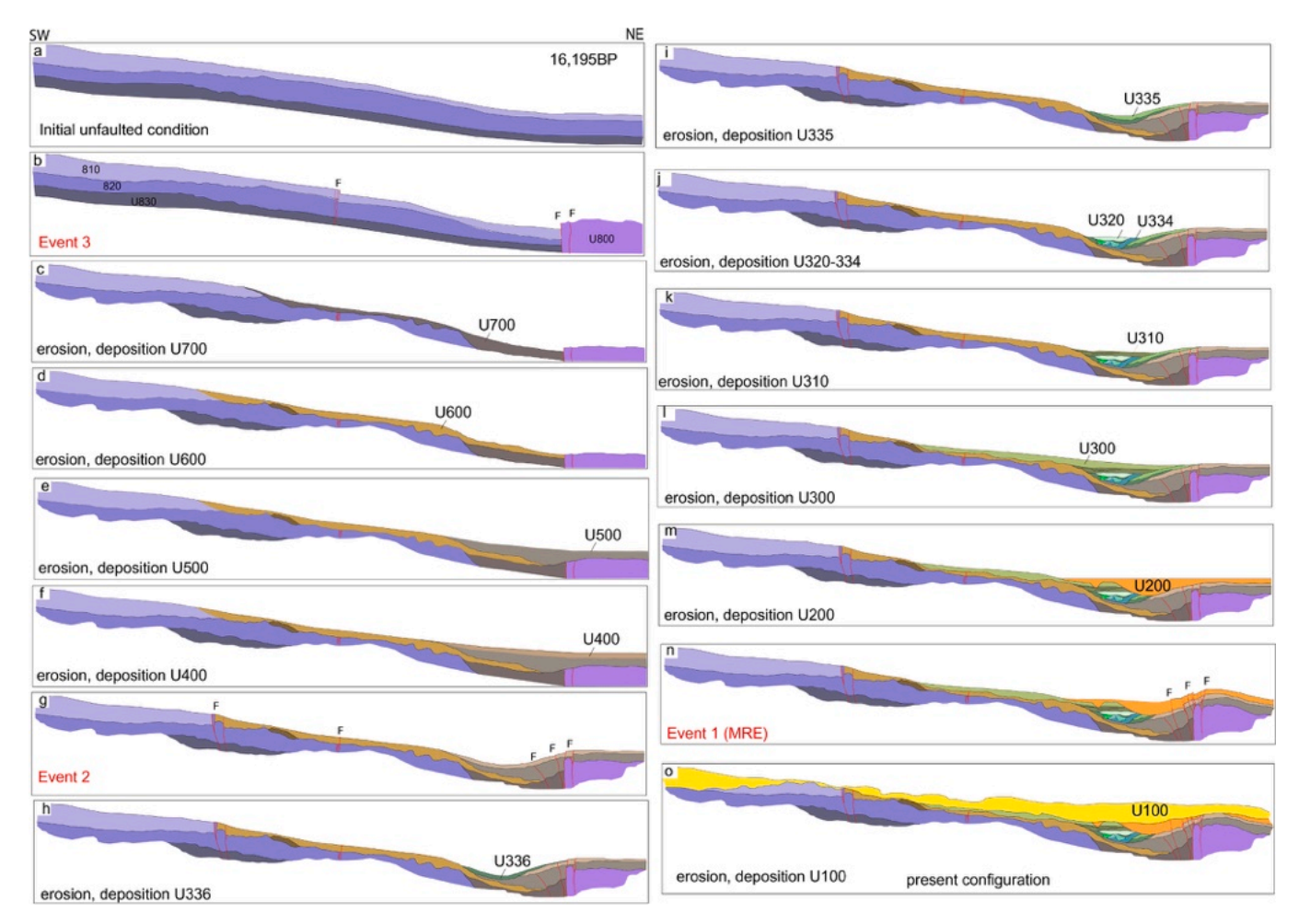


Fig. 18. Schematic reconstruction of faulting and depositional events observed in Trench 1. The sequence illustrates three interpreted ground-rupturing earthquakes based on cross-cutting relationships and unit correlations. This model supports the paleoseismic event chronology inferred from trench analysis. Note that the starting panel assumes an undeformed state prior to the events documented in the trench. This assumption is made for clarity in illustrating the sequence of identified earthquakes, but it should not be taken to imply an absence of earlier faulting. The reconstruction should be viewed as a schematic representation of the late-stage history captured in the exposed stratigraphy.

Table 2
Summary of radiocarbon dates from Trench 1.

Events	Units	Sample number	Material	Trench panel	C14 age (BP)	1Sigma	Comments
	100	KNG-12	Peat	18	390	20	Youngest stratigraphy in the trench
	100	KNG-3	Peat	25	380	20	
E1							
	300	KNG-15	Charcoal	13	300	20	
E2							
	400	KNG-27	Charcoal	27	415	20	
	432	KNG-7	Charcoal	21	840	20	Reworked charcoal
	500	KNG-25	Charcoal	25	720	20	
	500	KNG-4	Charred wood	22	990	20	
E3							
	820	KNG 19	Charred wood	4	16,350	20	Oldest strata exposed in the trench, within Weathered volcanic breccia
	830	KNG-22		10	16,195	20	Oldest strata exposed in the trench, within Weathered volcanic breccia

Note. Bold text indicates samples that are included in the age model calculation for the earthquake events. Samples were dated at the W. M. Keck Carbon Cycle Accelerator Mass Spectrometry Laboratory at the University of California, Irvine.

Faults observed in Panel 8–9 of Trench 1 (Fig. 14) offset Units 810 and 600 and are capped by the erosional surface at the base of U100. Because U100 truncates across these older units and no overlying stratigraphy is preserved, the timing of faulting cannot be attributed with confidence to E3, E2, or E1. These structures are therefore classified as undifferentiated faulting predating U100 deposition, reflecting the limitation of the preserved stratigraphic record. U600 is interpreted as a

single debris-flow or mass-flow deposit with a sharp basal contact and no clear internal stratification. Because the fault strand terminates at the base of U600, the faulting is interpreted to postdate its deposition, making E2 or E1 the most likely events. However, because the upper surface of U600 is irregular and locally eroded, we cannot fully exclude the possibility that subtle deformation is not expressed in the preserved exposure.

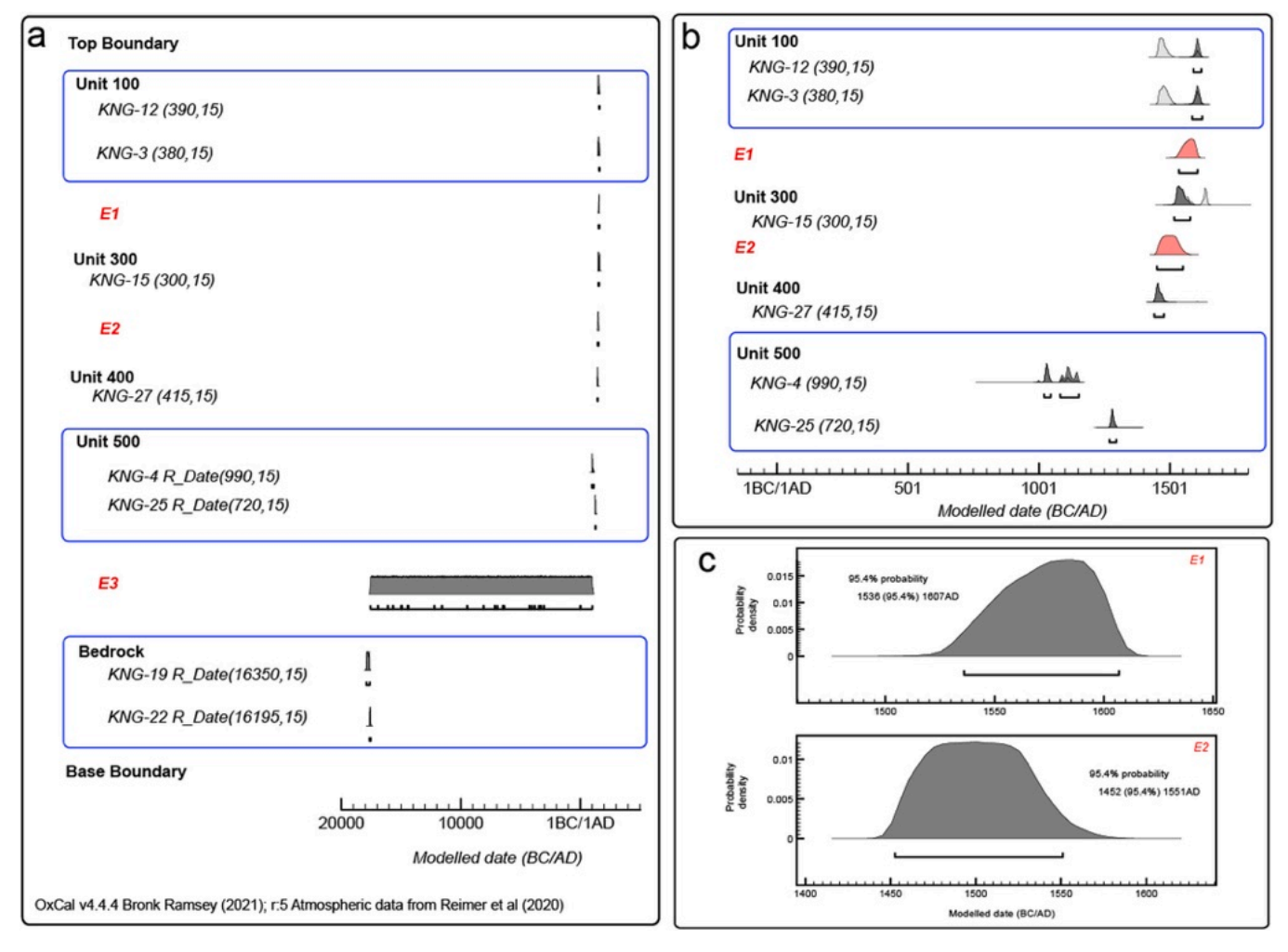


Fig. 19. (a) Radiocarbon age model derived from T1 charcoal samples, processed using OxCal v4.4 software (Ramsey, 2009). Calibrated age ranges (R_Date) follow the IntCal13 curve (Reimer et al., 2013). Paleoseismic event horizons (E1–E3) are constrained by bracketing units. Darker portions of the probability density functions indicate stratigraphically-constrained age intervals. (b) Enlarged view of the age model for earthquake events E1–E2, bounded by the age of Unit 400 at the base and Unit 100 at the top. (3) Detailed view of the resolved age model for earthquake events E1 and E2.

The fault strand in Panel 14 offsets Units 820 and 600 and is capped by the erosional surface at the base of U300. The exposure quality and upward termination are insufficient to confidently determine whether the faulting corresponds to E3 (pre-U600) or E2 (post-U600). Given the small amount of vertical separation and poor preservation of the upper contact, this feature is interpreted as undifferentiated pre-U300 faulting, providing weak evidence for event assignment.

We note, however, that our reconstruction of fault activity (Fig. 18) necessarily simplifies the long-term structural history. In particular, the starting panel assumes an undeformed state prior to the events documented in the trench. This assumption is made for clarity in illustrating the sequence of identified earthquakes, but it should not be taken to imply an absence of earlier faulting. The contact between Unit 820 and Unit 700 is erosional, indicating incision into the older weathered profile (Units 800-810) prior to the deposition of colluvial materials that make up Unit 700. Subsequent stream activity is recorded by Units 336-300, which further modified the underlying sequence. This geometry is best explained by vertical separation associated with lateral translation, rather than vertical displacement, and does not correspond to a small pull-apart structure or sag pond. Considering the age of the volcanic basement, the published slip rates, and the paleoseismic evidence for one or two ruptures in recent centuries, it is highly unlikely that deformation has been limited to the events documented here. Instead, our reconstruction should be viewed as a schematic

representation of the late-stage history captured in the exposed stratigraphy.

4.2.4.3. Chronological constraints on events. The relative timing of these paleoearthquakes was constrained through a combination of stratigraphic relationships and radiocarbon dating of organic materials (charcoal and wood) embedded within key sedimentary units (Table 2). A Bayesian chronological model was developed using OxCal software (Ramsey, 2009; Lienkaemper and Ramsey, 2009) to integrate the radiocarbon data with stratigraphic context and to estimate the most likely timing of each event Fig. 19). Radiocarbon dates from the same stratigraphic horizon were grouped using Phase in OxCal, as they represent coeval deposition within a single unit.

Event E1, which deforms Unit 200 and is overlain by undeformed Unit 100, is estimated to have occurred around 1573 \pm 34 CE. Event E2, which postdates Unit 400 and predates Units 336 to 310, is dated to 1452–1551 CE. The earliest event, E3, remains poorly constrained due to the scarcity of datable material in the lower portion of the trench. The modeled age range for E3 spans from 1767 BCE–1018 CE, highlighting considerable uncertainty in its timing.

Together, the ages of Events E1 through E2 indicate that two significant surface-rupturing earthquakes occurred within a relatively short period of a few decades to ~ 155 years. This suggests a potentially active seismic cycle during the Holocene that warrants further investigation.

5. Discussions

Our trench exposures reveal clear evidence for at least three surface-rupturing earthquakes since 1767–17,528 BCE, based on repeated fault terminations and event horizons cutting multiple stratigraphic units. However, the age control for the oldest event (E3) is limited due to the scarcity of organic materials suitable for radiocarbon dating in the lower stratigraphy. Consequently, the age model for this event remains poorly constrained. In contrast, the two younger events (E1 and E2) are built by multiple radiocarbon dates obtained from abundant charcoal and wood fragments, allowing for a more robust temporal reconstruction of the earthquake sequence.

Our age model for the two most recent events (E1 and E2) is constrained by their relationship to dated stratigraphic units. The age constraints for E1 and E2 rely heavily on a single radiocarbon date from Unit 300 (aged 1518-1578 CE), which lies between the two events. Event E2 does not rupture Unit 300, implying it predates its deposition, whereas Event E1 displaces the overlying Unit 200 but not Unit 100, which provides a maximum limiting age for E1. The calibrated age ranges for E1 (1539-1607 CE) and E2 (1452-1551 CE) overlap, with a common interval of 1539-1551 CE. Based on ages alone, it is not possible to unambiguously separate these two events. However, the trench stratigraphy shows that E1 and E2 rupture distinct stratigraphic horizons, making it more plausible that they represent two earthquakes occurring relatively close in time rather than a single rupture represented by overlapping calibrated ranges. Importantly, Unit 300 exhibits multiple scouring and depositional episodes, indicating that it likely represents at least a modest time interval of fluvial activity between the two rupture events, rather than rapid deposition during a single shortlived event. This temporal gap supports the interpretation of E1 and E2 as separate earthquakes rather than a doublet or mainshock-aftershock sequence. Because detrital charcoal from Units 300 and 100 may contain inherited ages, the E1 age is interpreted as a maximum age constraint, rather than a precisely bounded depositional age based solely on the calibrated pdf. This approach accounts for the possibility that some dated material predates deposition, reducing the likelihood of over-interpreting the temporal overlap with E2. Nonetheless, the combination of stratigraphic relationships and sedimentary evidence provides a reasonable basis to interpret E1 and E2 as distinct events.

The third, older event predates the well-dated stratigraphy and is broadly constrained to 1767 BCE–1018 CE due to limited datable material. Another issue pertains to the interpretation of stratigraphic boundaries within weathered bedrock. In our study, the volcanic breccia unit exhibited a weathering profile that mimicked stratigraphic layering. The U810–U820 contact reflects a weathering front developed within the volcanic breccia, not a structural surface. The weathering rind is more pronounced near the surface due to prolonged exposure to meteoric processes and becomes less developed with increasing depth. Because this weathering front tends to mimic the scarp geometry, it can create an apparent layering that, without careful analysis, might be misinterpreted as folding or as a separate depositional unit. This highlights the importance of integrating lithological observations with stratigraphic context to distinguish in-situ weathered bedrock from true sedimentary layering.

Because the two most recent events have overlapping calibrated age ranges and the older event has large age uncertainty, the available data do not provide sufficiently constrained event separation to calculate a robust mean recurrence interval. While a separation of up to $\sim\!155$ years between E1 and E2 would be geologically reasonable for a fault with a slip rate of $\sim\!30$ mm/yr, the broad uncertainty and the possibility that these events may represent a single rupture or closely spaced doublet make any recurrence calculation potentially misleading. Reporting a numerical recurrence interval in this context would understate the true uncertainty associated with the age data.

Results from our study indicate that the Aceh Fault has generated at

least three surface-rupturing earthquakes in the late Holocene to historical period. Although several moderate-magnitude earthquakes have occurred along the Aceh Fault in recent decades, such as the M4.8 event on June 4, 2020, and the M5.9 event on January 22, 2013—there are, to our knowledge, no well-documented accounts of large surface-rupturing earthquakes along this section of the fault in the historical or instrumental records. The absence of such records may reflect either the relatively low frequency of large events, the limited historical documentation and seismic monitoring in the region, or the possibility that part of the deformation is accommodated aseismically through fault creep. We also note that historical archival research for this region, particularly for the 16th century and later, remains incomplete, and additional investigations of colonial and regional sources (e.g., Dutch archives) may yet reveal overlooked accounts of large earthquakes. The most recent event identified in the trench (E1), dated to around 1573 \pm 34 CE, occurred prior to the establishment of reliable instrumental records and likely predates the available historical archives. This indicates that more than 400 years have elapsed since the last documented rupture at this site, implying that significant seismic hazard remains unrecognized along this section of the Aceh Fault.

This temporal gap, combined with the absence of historically documented surface ruptures in the region, raises several important considerations. One possibility is that some of the paleoearthquake events identified in the trench, particularly the older ones, may represent moderate-magnitude earthquakes (e.g., M5–6) capable of producing localized surface rupture. We do not assume a regular recurrence pattern between events—for example, the interval between E1 and E2 could have been relatively short, whereas the open interval may reflect a much longer period of quiescence. Rather, our point is that even smaller-magnitude events can occasionally leave a recognizable stratigraphic signature, as documented elsewhere (e.g., Liu-Zeng et al., 2007, in China), and should therefore be considered when interpreting incomplete or irregular paleoseismic records.

Second, the lack of recent surface rupture despite the elapsed time may be partially explained by the presence of aseismic creep along portions of the fault. Geodetic and geomorphic studies in parts of the Sumatran fault system suggest that some segments may accommodate strain through creep, thereby reducing the accumulation of elastic strain and delaying the recurrence of larger seismic events. If a significant portion of deformation is being released aseismically, then some of the events observed in the trench may not correspond to large-magnitude earthquakes, and the overall seismic moment release over time may be lower than implied by the paleoseismic record alone. Our trench is located within the creeping section of the Aceh Fault, where InSAR data show surface creep rates of up to \sim 20 mm/yr along a \sim 100 km stretch of the fault (Tong et al., 2018). If creep were expressed at the ground surface, we would expect to see subtle or distributed deformation extending through the upper stratigraphic units, particularly unit 100. No such deformation was observed in the trench, suggesting either that (1) shallow deposits locally mask or absorb the signal of aseismic slip, (2) creep is occurring at depth but is not expressed in the surficial layers, or (3) this portion of the fault accommodates creep heterogeneously. This absence is itself important for understanding how aseismic slip may vary spatially along the creeping section of the fault.

These factors together suggest that the trench record may reflect a mix of event sizes, including moderate earthquakes and possibly even deformation events associated with slow slip or creep-related processes. Overestimating the frequency of large-magnitude earthquakes based solely on stratigraphic evidence could mislead hazard assessments, particularly when such a recurrence rate exceeds what is observed in historical or instrumental records.

Therefore, we emphasize that the recurrence interval derived from stratigraphic records represents a minimum constraint and should be considered within the broader tectonic and seismotectonic context, which includes the potential for aseismic deformation and variable earthquake magnitudes. Additional studies integrating geodesy, fault

slip rate estimates, and other trench sites along this segment are essential to better characterize the fault behavior and its implications for regional seismic hazard. Additional trenches, targeted sampling of undisturbed fine-grained units, and application of independent dating methods (e.g., OSL, tephrochronology) are necessary to refine event ages, increase event count, and allow a robust recurrence analysis in the future.

Importantly, our results confirm active seismic deformation along this previously understudied section of the Aceh Fault and provide the first direct paleoseismic evidence of surface-rupturing earthquakes along this portion of the Great Sumatran Fault system. This represents a significant advancement in our understanding of seismic hazards in the region and highlights the critical need for further paleoseismic investigations along other unstudied sections of the fault.

In summary, while this study provides essential new data on the paleoseismic behavior of the Aceh Fault, it also illustrates the methodological and environmental challenges associated with conducting paleoseismic research in tropical, high-rainfall environments. Addressing these challenges through improved site selection and multidisciplinary integration will be crucial for building a more comprehensive seismic hazard model for northern Sumatra and beyond.

6. Conclusions

In this study, we present new results from active fault mapping and paleoseismic investigations along the Aceh segment of the Sumatran Fault. Through detailed geomorphic analysis and field observations, we have refined the surface trace of the Aceh Fault and delineated its geometry with greater resolution than previously available. We provide a KML file containing the fault mapping as an electronic supplement to the manuscript. Furthermore, our interpretation of offshore bathymetric data extends the trace of the fault an additional 60 km to the northwest, beyond Pulo Aceh. This extension significantly increases the total length of the Aceh Fault, thereby raising its maximum earthquake magnitude potential and highlighting the importance of this section in regional seismic hazard assessments.

We also report the first paleoseismological evidence of past surfacerupturing earthquakes along this fault section. Trenching investigations revealed a stratigraphic record of three ground-rupturing events within the upper two meters of deposits, representing approximately the last 1000 years of sedimentation. The youngest two events are supported by robust radiocarbon dating, while the oldest require further chronological refinement. These findings confirm that the Aceh Fault is tectonically active and capable of producing surface-rupturing earthquakes.

Although the age constraints do not allow us to resolve all three events with high precision, the stratigraphic evidence alone is sufficient to confirm that the Aceh Fault has generated at least three surface-rupturing earthquakes in the late Holocene to historical period. This is a significant finding for the seismic history of the region, given the scarcity of direct paleoseismic observations along this segment.

CRediT authorship contribution statement

Gayatri Indah Marliyani: Writing – review & editing, Writing – original draft, Visualization, Validation, Supervision, Software, Resources, Project administration, Methodology, Investigation, Funding acquisition, Formal analysis, Data curation, Conceptualization. Yann Klinger: Writing – review & editing, Writing – original draft, Validation, Methodology, Formal analysis, Data curation, Conceptualization. Aulia Kurnia Hady: Visualization, Validation, Methodology, Data curation. Agung Setianto: Visualization, Methodology, Data curation. Wenqian Yao: Writing – original draft, Methodology, Formal analysis, Data curation. Hurien Helmi: Visualization, Software, Investigation, Formal analysis, Data curation, Conceptualization. Telly Kurniawan: Software, Methodology, Investigation, Funding acquisition, Data curation. Retno Agung Prasetyo Kambali: Project administration, Funding acquisition,

Conceptualization. Zulham Sugito: Resources, Project administration, Investigation, Data curation. Abdi Jihad: Resources, Project administration, Data curation. Yosi Setiawan: Visualization, Software, Methodology, Data curation. Andi Azhar Rusdin: Resources, Project administration, Investigation, Data curation. Jimmi Nugraha: Resources, Project administration, Investigation, Data curation. Supriyanto Rohadi: Resources, Project administration, Funding acquisition, Conceptualization. Rahmat Triyono: Supervision, Resources, Project administration, Funding acquisition, Formal analysis, Conceptualization. Dwikorita Karnawati: Supervision, Project administration, Funding acquisition, Funding acquisition, Conceptualization.

Declaration of competing interest

The authors declare that they have no known competing financial interests or personal relationships that could have appeared to influence the work reported in this paper.

Data availability

Data will be made available on request.

Acknowledgements

This study was supported by the Meteorology, Climatology, and Geophysics Agency of Indonesia (BMKG); the PHC Nusantara Grant as part of the Sustainable Development Research Funding Program – International Collaboration Scheme (Program Pendanaan Riset Pembangunan Berkelanjutan Skema Kerja Sama Luar Negeri, PPRPB-KLN), funded by the Indonesian Endowment Fund for Education (LPDP) and the French National Centre for Scientific Research (CNRS). The early phase of this research was also supported by funding from the State University Operational Assistance Program (Bantuan Operasional Perguruan Tinggi Negeri, BOPTN) of the Ministry of Education, Science, and Technology of Indonesia. We thank Kate Scharer and the anonymous reviewers for their constructive comments and suggestions, which have improved this paper. We are also grateful to Yugi Cahya Fardana and Ahmad As'at Abhista for their valuable assistance during fieldwork.

References

- Bellier, O., Sebrier, M., 1995. Is the slip rate variation on the Great Sumatran Fault accommodated by fore-arc stretching? Geophys. Res. Lett. 22 (15), 1969–1972.
 Bellier, O., Sebrier, M., Pramumijoyo, S., Beaudouin, T., Harjono, H., Bahar, I., Forni, O., 1997. Paleoseismicity and seismic hazard along the Great Sumatran Fault (Indonesia). J. Geodyn. 24 (1–4), 169–183.
- Bennett, J.D., Bridge, D.M., Cameron, N.R., Djunuddin, A., Ghazali, S.A., Jeffery, D.H., Kartawa, W., Keats, W., Rock, N.M.S., Thomson, S.J., Whandoyo, R., 1981. Geologic Map of the Banda Aceh Quadrangle, Sumatra. Geol. Res. Dev. Cent, Bandung, Indonesia.
- Berglar, K., Gaedicke, C., Ladage, S., Thoele, H., 2017. The Mentawai forearc sliver off Sumatra: a model for a strike-slip duplex at a regional scale. Tectonophysics 710, 225–231.
- Bock, Y., Prawirodirdjo, L., Genrich, J.F., Stevens, C.W., McCaffrey, R., Subarya, C., Puntodewo, S.S.O., Calais, E., 2003. Crustal motion in Indonesia from global positioning system measurements. J. Geophys. Res.: SolidEarth 108 (B8).
- Bonilla, M.G., Lienkaemper, J.J., 1991. Factors Affecting the Recognition of Faults Exposed in Exploratory Trenches (no. 1947). US Government Printing Office
- Curray, J.R., Moore, D.G., Lawver, L.A., Emmel, F.J., Raitt, R.W., Henry, M., Kieckhefer, R., 1979. Tectonics of the Andaman Sea and Burma: Convergent Margins.
- DeMets, C., Gordon, R.G., Argus, D.F., Stein, S., 1990. Current plate motions. Geophys. J. Int. 101 (2), 425–478.
- Diament, M., Harjono, H., Karta, K., Deplus, C., Dahrin, D., Zen Jr., M.T., Gerard, M., Lassal, O., Martin, A., Malod, J., 1992. Mentawai fault zone off Sumatra: a new key to the geodynamics of western Indonesia. Geology 20 (3), 259–262.
- Genrich, J.F., Bock, Y., McCaffrey, R., Prawirodirdjo, L., Stevens, C.W., Puntodewo, S.S. O., Subarya, C., Wdowinski, S., 2000. Distribution of slip at the northern Sumatran fault system. J. Geophys. Res. Solid Earth 105 (B12), 28327–28341.
- Guzmán-Speziale, M., 2024. Oblique plate convergence along arcuate trenches on a spherical Earth. An example from the Western Sunda Arc. Acta Geophys. 72 (1), 7–27.

- Hady, A.K., 2020. Geometri Dan Segmentasi Sesar Aceh (5.38 derajat N, 95.8 derajat E sampai 4.38 derajat N, 96.16 derajat E) Daerah Nagan Raya, Pidie, Dan Aceh Besar. Master thesis, Universitas Gadjah Mada.
- Hady, A.K., Marliyani, G.I., 2020. Updated Segmentation Model of the Aceh Segment of the Great Sumatran Fault System in Northern Sumatra, Indonesia. J. Appl. Geol. 5 (2), 84–100.
- Ito, T., Gunawan, E., Kimata, F., Tabei, T., Simons, M., Meilano, I., Agustan, Ohta, Y., Nurdin, I., Sugiyanto, D., 2012. Isolating along-strike variations in the depth extent of shallow creep and fault locking on the northern Great Sumatran Fault. J. Geophys. Res. Solid Earth 117 (B6). https://doi.org/10.1029/2011JB008940.
- Jourdain, A., Singh, S.C., Escartin, J., Klinger, Y., Raju, K.K., McArdle, J., 2016. Crustal accretion at a sedimented spreading center in the Andaman Sea. Geology 44 (5), 351–354.
- Kreemer, C., Holt, W.E., Haines, A.J., 2003. An integrated global model of present-day plate motions and plate boundary deformation. Geophys. J. Int. 154 (1), 8–34.
- Lienkaemper, J.J., Ramsey, C.B., 2009. OxCal: Versatile tool for developing paleoearthquake chronologies—a primer. Seismol. Res. Lett. 80 (3), 431–434.
- Liu-Zeng, J., Klinger, Y., Xu, X., Lasserre, C., Chen, G., Chen, W., Tapponnier, P., Zhang, B., 2007. Millennial recurrence of large earthquakes on the Haiyuan fault near Songshan, Gansu Province, China. Bull. Seismol. Soc. Am. 97 (1B), 14–34.
- Marliyani, G.I., Grant, L.G., 2016. Trenching as a method of paleoseismological data collection: improved techniques and applications. Appl. Geol. California 1000. Anderson, R. and Ferriz, H., (eds.), 2016.
- McCaffrey, R., 2009. The tectonic framework of the Sumatran subduction zone. Annu. Rev. Earth Planet. Sci. 37, 345–366.
- McCaffrey, R., Zwick, P.C., Bock, Y., Prawirodirdjo, L., Genrich, J.F., Stevens, C.W., Puntodewo, S.S.O., Subarya, C., 2000. Strain partitioning during oblique plate convergence in northern Sumatra: Geodetic and seismologic constraints and numerical modeling. J. Geophys. Res. Solid Earth 105 (B12), 28363–28376.
- McCalpin, J., Ferrario, F., Figueiredo, P., Livio, F., Grützner, C., Pisarska-Jamroży, M., Quigley, M., Reicherter, K., Rockwell, T., Štěpančíková, P., Tábořík, P., 2023. New developments in onshore paleoseismic methods, and their impact on Quaternary tectonic studies. Quat. Int. 664, 59–76.
- Mignan, A., Danciu, L., Giardini, D., 2015. Reassessment of the maximum fault rupture length of strike-slip earthquakes and inference on M max in the Anatolian Peninsula, Turkey. Seismol. Res. Lett. 86 (3), 890–900.
- Moechtar, H., Subiyanto, S., Sugianto, D., 2009. Geologi aluvium dan karakter endapan pantai/pematang pantai di Lembah Krueng Aceh, Aceh besar (prov. NAD). J. Geologi dan Sumberdaya Min. 19 (4), 273–283.
- Natawidjaja, D.H., Bradley, K., Daryono, M.R., et al., 2017. Late Quaternary eruption of the Ranau Caldera and new geological slip rates of the Sumatran Fault Zone in

- Southern Sumatra, Indonesia. Geosci. Lett. 4, 21. https://doi.org/10.1186/s40562-017-0087-2.
- Pedersen, N.B., Björdal, C.G., Jensen, P., Felby, C., 2012. Bacterial Degradation of Archaeological Wood in Anoxic Waterlogged Environments.
- Pinzon, N., Klinger, Y., Xu, X., Tapponnier, P., Liu-Zeng, J., Van Der Woerd, J., Li, K., Gao, M., 2024. Spatiotemporal Clustering of large Earthquakes along the Central-Eastern Sections of the Altyn Tagh Fault, China. J. Geophys. Res. Solid Earth 129 (12), e2024JB028912.
- Pusat Studi gempa Nasional, 2017. Peta Sumber dan Bahaya Gempa Bumi Indonesia Tahun 2017. Badan Penelitian dan Pengembangan Kementerian PUPR.
- Ramsey, C.B., 2009. Bayesian analysis of radiocarbon dates. Radiocarbon 51 (1), 337–360.
- Reimer, P.J., 2020. Composition and consequences of the IntCal20 radiocarbon calibration curve. Quatern. Res. 96, 22–27.
- Reimer, P.J., Bard, E., Bayliss, A., Beck, J.W., Blackwell, P.G., Ramsey, C.B., Brown, D. M., Buck, C.E., Edwards, R.L., Friedrich, M., Grootes, P.M., 2013a. Selection and treatment of data for radiocarbon calibration: an update to the International Calibration (IntCal) criteria. Radiocarbon 55 (4), 1923–1945.
- Reimer, P.J., Bard, E., Bayliss, A., Beck, J.W., Blackwell, P.G., Ramsey, C.B., Buck, C.E., Cheng, H., Edwards, R.L., Friedrich, M., Grootes, P.M., 2013b. IntCall3 and Marine13 radiocarbon age calibration curves 0–50,000 years cal BP. Radiocarbon 55 (4), 1869–1887.
- Rofi, A., Doocy, S., Robinson, C., 2006. Tsunami mortality and displacement in Aceh province, Indonesia. Disasters 30 (3), 340–350.
- Sieh, K., & Natawidjaja, D. (2000). Neotectonics of the Sumatran fault, Indonesia. J. Geophys. Res., 105, 28,295–28,326. doi:https://doi.org/10.1029/2000JB900120.
- Singh, S.C., Moeremans, R., McArdle, J., Johansen, K., 2013. Seismic images of the sliver strike-slip fault and back thrust in the Andaman-Nicobar region. J. Geophys. Res. Solid Earth 118 (10), 5208–5224.
- Tong, X., Sandwell, D.T., Schmidt, D.A., 2018. Surface creep rate and moment accumulation rate along the Aceh segment of the Sumatran fault from L-band ALOS-1/PALSAR-1 observations. Geophys. Res. Lett. 45 (8), 3404–3412.
- Tregoning, P., 2002. Plate kinematics in the western Pacific derived from geodetic observations. J. Geophys. Res. Solid Earth 107 (B1), ECV-7.
- Tsutsumi, H., Soeda, Y., Ismail, N., Ali, B., Tabei, T., 2022. Tectonic landform and paleoseismic activity of the northernmost Sumatran Fault. Authorea Preprints, Aceh province. Indonesia.
- Walker, M., 2005. Quaternary Dating Methods. John Wiley and Sons.
- Yanis, M., Islami, G., Ismail, N., 2022. Geophysics and geomorphic observation for nearsurface structures mapping of Seulimeum Fault on Lamtamot area, Northern Sumatra. Bullet. Geol. Soc. Malaysia 73. https://doi.org/10.7186/bgsm73202211.